

Tidal Downsizing Model. III. Planets from sub-Earths to Brown Dwarfs: structure and metallicity preferences

Sergei Nayakshin and Mark Fletcher

Department of Physics & Astronomy, University of Leicester, Leicester, LE1 7RH, UK

E-mail: Sergei.Nayakshin@le.ac.uk

Received

ABSTRACT

We present population synthesis calculations of the Tidal Downsizing (TD) hypothesis for planet formation. Our models address the following observations: (i) most abundant planets being Super Earths; (ii) cores more massive than $\sim 5 - 15M_{\oplus}$ are enveloped by massive atmospheres; (iii) the frequency of occurrence of close-in gas giant planets correlates strongly with metallicity of the host star; (iv) no such correlation is found for sub-Neptune planets; (v) presence of massive cores in giant planets; (vi) gas giant planets are over-abundant in metals compared to their host stars; (vii) this over-abundance decreases with planet's mass; (viii) a deep valley in the planet mass function between masses of $\sim 10 - 20M_{\oplus}$ and $\sim 100M_{\oplus}$. A number of observational predictions distinguish the model from Core Accretion: (a) composition of the massive cores is always dominated by rocks not ices; (b) the core mass function is smooth with no minimum at $\sim 3M_{\oplus}$ and has no ice-dominated cores; (c) gas giants beyond 10 AU are insensitive to the host star metallicity; (d) objects more massive than $\sim 10M_{\text{Jup}}$ do not correlate or even anti-correlate with metallicity. The latter prediction is consistent with observations of low mass stellar companions. TD can also explain formation of planets in close binary systems. TD model is a viable alternative to the Core Accretion scenario in explaining many features of the observed population of exoplanets.

1 INTRODUCTION

Core Accretion model (CA; e.g., Pollack et al. 1996; Alibert et al. 2005) stipulates that all planets grow from planetesimals – rocky or icy bodies ~ 1 km or more in size (Safronov 1972). Planetesimals combine into bigger solid bodies by sticking collisions. More recent work suggests that planetesimals may have formed via streaming instabilities (Youdin & Goodman 2005; Johansen et al. 2007) and were born big, e.g., as large as ~ 100 to 1000 km in size (Morbidelli et al. 2009). In addition to this, pebbles, which are grains that have grown to the size of ~ 1 mm to a few cm, are now suspected to contribute to the growth of the cores strongly (Ormel & Klahr 2010; Lambrechts & Johansen 2012; Chambers 2014; Lambrechts et al. 2014).

Whatever the growth mechanism of the cores, those that become massive attract gaseous atmospheres from protoplanetary discs. The atmosphere eventually becomes as massive as the core when the core mass exceeds a critical value, $M_{\text{crit}} \sim 10 M_{\oplus}$, although the exact critical core mass is a function of dust opacity, planet's location and other important physics (e.g., Perri & Cameron 1974; Mizuno 1980; Stevenson 1982; Rafikov 2006). At this point a runaway accretion of gas onto the core takes place, forming a gas giant planet (Pollack et al. 1996; Hubickyj et al. 2005).

CA is the most widely accepted theory of planet formation (e.g., see Helled et al. 2013). CA popularity is motivated by its successes and, in no small measure, by the

failures of the alternative model, Gravitational disc Instability (GI; e.g., Kuiper 1951; Cameron et al. 1982; Boss 1997). In particular, the classical version of GI cannot account for (i) the existence of terrestrial/rocky planets; (ii) any planets within the inner \sim tens of AU of the host star; (iii) presence of massive cores inside of and metal overabundance of gas giant planets, and (iv) a positive giant planet frequency of occurrence – host star metallicity correlation (Fischer & Valenti 2005). CA, in contrast, has features (i–iii) built in by construction and predicts (iv) naturally as a result of producing more massive cores in high metallicity environments, so that the runaway gas accretion phase commences earlier (Ida & Lin 2004a,b; Mordasini et al. 2014).

However, a new planet formation framework called Tidal Downsizing (TD), in which GI is only the first step, has been suggested relatively recently (Boley et al. 2010; Nayakshin 2010a). The theory is an offspring of the Gravitational disc Instability model for planet formation (e.g., Cameron et al. 1982; Boss 1997) but is far richer in terms of physics included in it. In a way, TD theory is GI theory modernised by physical processes many of which became standard features of CA at various times, but were somehow forgotten to be included in GI. These processes are planet migration, solids coagulating into massive bodies, pebble accretion, and fragment disruption when compromised by too strong tidal forces from the host star. For a recent review of issues surrounding TD and GI, see Helled et al. (2013),

and section 2 in Nayakshin (2015d), the latter specifically focused on TD.

Several ways of addressing problems (i-iii) in the context of TD were qualitatively clear from its inception, but it is only very recently that a process accounting for (iv) was found. We have recently developed detailed population synthesis models of the new scenario enabling quantitative comparisons to observations. This paper, third in a series, presents a number of such comparisons and makes observational predictions that may discriminate between CA and TD in the future.

The origins of this new theory lie in the apparently forgotten suggestion of Kuiper (1951) that GI may form not only the gas giant planets of the Solar System but also the rocky ones. He suggested that the inner Solar System planets are made by destroying \sim Jupiter mass gas fragments within which dust sedimented down (McCrea & Williams 1965; Boss 1998) to form massive and dense cores composed of heavy elements. Hydrogen/helium and other volatile components of the fragments are disrupted by the Solar tides and eventually consumed by the Sun, whereas the much denser cores survive to become the present day planets.

Until Boley et al. (2010), no physical way of actually placing the massive gas fragments at \sim a few AU distances from the Sun seemed to exist (e.g., Rice et al. 2005; Rafikov 2005). This appears to be the main reason why this avenue of planet formation was discounted early on (Donnison & Williams 1975). However, we now know that the fragments do not have to be born where the planets are now because of planet migration (e.g., Lin & Papaloizou 1979; Goldreich & Tremaine 1980). Boley et al. (2010) found that \sim Jupiter mass gas fragments born by gravitational instability in the outer ($R \sim 100$ AU) cold protoplanetary disc do not stay there, as usually assumed, but migrate inward rapidly (in as little as $\sim 10^4$ yrs; see also Baruteau et al. 2011; Cha & Nayakshin 2011; Zhu et al. 2012). The fragments are initially very fluffy, and it takes up to a few Myrs (e.g., Bodenheimer 1974; Bodenheimer et al. 1980; Vazan & Helled 2012) for them to contract and collapse to what is usually taken as the time $t = 0$ configuration of GI planets (the so called "hot start" of gas giants, see, e.g., Marley et al. 2007). Since migration process is much quicker, the pre-collapse gas fragments are usually disrupted by tides from their host stars when the fragment separation shrinks to a few AU. Nayakshin (2010a) arrived at similar ideas via analytical estimates and simulations of core formation within isolated gas fragments (Nayakshin 2010b, 2011).

Since then, several dozen investigations into the physics of TD or into processes important to TD (cf. further references in Helled et al. 2013; Nayakshin 2015d) sprung up. There was however much less work on trying to relate the TD hypothesis to the observations of exoplanets in a quantitative way, which is not particularly surprising given the theory is still in its infancy. Nevertheless, Forgan & Rice (2013) and Galvagni & Mayer (2014) built the first population synthesis models for TD in order to compare the predictions of the models with the statistics of observed exoplanets (for the latter, see a recent review by Winn & Fabrycky 2014). The results of these two studies are somewhat divergent. Forgan & Rice (2013) find that TD is incapable of producing any planets at small separations ($R \lesssim 10$ AU) since most of

their gas fragments are tidally disrupted *before* massive solid cores could form within them. Galvagni & Mayer (2014) did not include grain sedimentation in their models, hence could not say anything about the post-disruption core-dominated planets. However, their study found a wealth of Jovian mass planets that successfully migrated into the inner disc, avoiding tidal disruptions, and hence they suggested that TD may well be effective in producing a hot-Jupiter like population of gas giants.

Another challenge to TD is the expectation that higher metallicity fragments are more likely to be tidally disrupted because of slower radiative cooling (Helled & Bodenheimer 2011). This would imply that low metallicity environments must be more hospitable to gas giant formation via TD channel. Since a strong positive giant planet frequency – metallicity correlation is observed (Gonzalez 1999; Fischer & Valenti 2005), the general feeling is that TD is strongly disfavoured by the data.

A solution to these and other shortcomings of TD hypothesis may be "pebble accretion" (Nayakshin 2015a), the process in which large (~ 1 mm to a few cm) grains from the disc separate out of the gas-dust flow past an embedded massive body (large planetesimal or a planet) and accrete onto it (e.g., Johansen & Lacerda 2010; Ormel & Klahr 2010; Lambrechts & Johansen 2012). Pebble accretion is mainly called upon in the Core Accretion model to accelerate the growth of solid cores at large distances (e.g., Helled & Bodenheimer 2014; Chambers 2014; Lambrechts et al. 2014); no application of pebble accretion to TD was however done until very recently.

A 1D radiative hydrodynamics study with grains treated as a second fluid showed that external pebble deposition in pre-collapse gas fragments significantly accelerates their contraction and collapse (Nayakshin 2015a). Using a 1D viscous disc evolution code to treat the disc-planet interactions (angular momentum and heat exchange, pebble accretion) and co-evolution, we confirmed that pebble accretion allows more fragments to survive tidal disruptions, and also does so preferentially in high metallicity environments (Nayakshin 2015b). In paper I (Nayakshin 2015d), this numerical scheme was extended to include grain growth, sedimentation and core formation within the fragments. In paper II (Nayakshin 2015c), a large set of population-synthesis like experiments in TD setting was performed. Since pebble accretion strongly increases grain and metal abundance within the gas fragments, massive ($M_{\text{core}} \sim 10 M_{\oplus}$) cores composed of heavy elements form much quicker than they do inside "pristine" fragments made of the dust/gas composition equal to that of the host star. For this reason, an abundant massive core presence in the inner disc was found in paper II, in contrast to the earlier results by Forgan & Rice (2013).

Interestingly, while survival of gas giant planets in these numerical experiments was strongly enhanced at high metallicities, the same was not true for core dominated planets with mass $\lesssim 10 M_{\oplus}$. These planets were most abundant around \sim Solar metallicity hosts rather than at higher metallicities. This result is in line with both radial velocity and transit observations of exoplanets (e.g., Sousa et al. 2008; Mayor et al. 2011; Buchhave et al. 2012) which showed that planets smaller than \sim Neptune in mass or radius do not correlate with metallicity of the host.

Strictly speaking, this contradicts expectations from CA (Ida & Lin 2004a) that massive cores are more abundant at high metallicities. This is the feature of the model called upon to explain the gas giant planet positive metallicity correlation with metal abundance of the host stars. While more recent work (Mordasini et al. 2012) shows that CA can explain the absence of metallicity correlation for Neptune mass or smaller planets, this result depends sensitively on uncertain details of type I migration prescription (see section 7.2 in the paper quoted just above).

Here we improve on methods of paper I and II in a number of ways, investigate the results in greater detail, and present additional model predictions to distinguish TD from CA observationally. First, we study a much broader range of the initial fragment masses, e.g., from the minimum of $M_{\min 0} = 1/3 M_J$ to the maximum of $M_{\max 0} = 16 M_J$ (Nayakshin 2015c, studied fragments in a much narrower mass range, $0.5 < M_0/M_J < 2$). This is important as the initial fragment mass cannot be accurately constrained at this stage: different authors arrive at different answers (e.g., Boley et al. 2010; Forgan & Rice 2011). Secondly, following Nayakshin et al. (2014), we calculate the structure of the dense gas layers adjacent to the core growing inside the gas fragment, hence resolving the gravitational influence of the core on the very centre of the gas fragment. This step is key to studying Neptune to \sim sub-Saturn mass planets. In the context of TD, such planets form when the core is surrounded by massive gas atmosphere *bound* to the core. This is physically similar to how massive gas atmospheres form around cores in the context of CA (e.g., Mizuno 1980; Stevenson 1982; Rafikov 2006), but all the action takes place in the centre of the massive gas fragment (formed by GI and not due to the presence of the core) rather than the protoplanetary disc. When the gas fragment is disrupted, the bound atmosphere survives together with the core since it is far denser than the rest of the fragment (Nayakshin et al. 2014). Finally, we now use a more realistic – better observationally constrained – approach to the protoplanetary disc dispersal to end our runs.

We find that our population synthesis model reproduces a number of observational facts/correlations for planetary properties that were previously suggested to vindicate CA as the only correct theory of planet formation, such as the metallicity correlations, the presence of cores inside of and the general overabundance of metals in gas giant planets compared to their host stars, the existence of a critical core mass above which the core must possess a massive envelope composed of volatiles and hydrogen/helium. Fortunately, there turn out to be a number of observational predictions distinguishing our theory from CA model.

Section 2 of this paper presents a summary of the main assumptions and numerical methods used here. Readers not interested in computational detail of the model may skip section 2 and proceed to §3, where a broad brush overview of the results is presented. Planet mass function (PMF), metallicity correlations, planet and core compositions are described in §4-9. The radial distribution of simulated planets is compared to observational constraints in §10. A broad discussion of the implications of the results is given in §11.

2 COMPUTATIONAL APPROACH

2.1 Main assumptions

Our main assumptions are very similar to those in paper I and II. We recount them briefly below, with more detail on the calculations to follow in §2.2 below.

(i) We study the migration of a gas fragment in an initially massive self-gravitating disc around a star with mass $M_* = 1 M_\odot$ in the last phase of the disc existence. The fragments are born at separation $a \sim 100$ AU where this process is allowed by physical conditions. During our simulations, the mass supply from the parent molecular cloud has ceased, and the disc mass monotonically decreases due to accretion on the star and the disc photo-evaporation. This approach neglects the earlier population of fragments born when the star was less massive for the sake of simplicity at this exploratory stage.

(ii) Only one fragment per disc is simulated. This is a serious shortcoming of the calculations as simulations of self-gravitating discs show formation of multiple fragments forming and interacting with each other (e.g., Boley et al. 2010; Cha & Nayakshin 2011; Meru 2013). We attempt to mitigate for this by variations in the initial parameters of the disc and in the fragment’s migration speed (see §2.2).

(iii) Planetesimals are neglected in this paper. These minor bodies are a side show in the context of TD, something that also happens during planet formation but is not a prerequisite to formation of any of the planets. Moreover, in TD planetesimals are formed by the proto-planets (that is, massive gas fragments) and not the other way around. Specifically, Nayakshin (2011) argued (in §7 of that paper) that environments inside massive gas fragments are both better and safer for solids to grow than the main body of the protoplanetary discs. Higher gas densities and self-gravity of the gas fragments provide high grain growth rates and protection against fragmenting high speed collisions, turbulence and the rapid migration of the fragments into the star (the famous “1 metre barrier”, see Weidenschilling 1980). Nayakshin & Cha (2012) showed that within the fragment, solid bodies with small angular momentum accrete onto the central massive core, whereas ~ 1 km or larger bodies with a larger angular momentum orbit the core instead. When the gas fragment is disrupted, bodies closest to the core remain bound to it, possibly contributing to formation of satellites of future super Earth or more massive planets. Bodies farther away from the core become gravitationally unbound from it when the fragment is disrupted. They however remain bound to the parent star and form debris rings with orbital properties not unlike the Kuiper and the asteroid belts (Nayakshin & Cha 2012). Most importantly, there is likely much less mass in these fragment-produced “planetesimals” than in the Core Accretion scenarios of planet formation. For this reason, although planetesimals formed in earlier generations of disrupted fragments may accrete onto and influence the gas fragment evolution (e.g., see Helled et al. 2008; Boley et al. 2011), this process is neglected in the present paper.

(iv) Once formed by gravitational instability, fragments do NOT accrete more gas from the disc. Nayakshin & Cha (2013) performed 3D SPH simulations of gas fragments embedded in massive marginally stable discs that included

a physically motivated analytical prescription for radiative heating of the gas around the planet’s location. It was found that planets less massive than $\sim 5 - 10$ Jupiter masses create a hot atmosphere around themselves that stifles accretion of more gas onto them. More massive planets accrete gas rapidly and run away well into the BD regime at which point migration of the fragment is stalled. More 3D simulations are needed to ascertain (in)dependence of this result on dust opacity of the disc and other parameters of the model.

(v) Pebbles are accreting onto the fragments at the rate (equation 5 in paper II) calculated by extrapolating results from Lambrechts & Johansen (2012). The size of the pebbles is set to 0.3 mm for simplicity, and the incoming pebbles are deposited into the outermost layers of the planet.

Readers not interested in technical details of the calculations may skip section 2.2 and continue directly to section 3 where results of this paper are beginning to be presented.

2.2 Summary of numerical methods

We follow numerical methods explained at length in paper I and II. These are summarised below. We also explain several important modifications that improve our methods.

2.2.1 Disc evolution

We set the inner boundary of the disc to $R_{\text{in}} = 0.08$ AU, whereas the outer boundary is set to $R_{\text{out}} = 400$ AU for this paper. We use 300 radial bins, logarithmically spaced in $R^{1/2}$, which gives us the highest numerical resolution near the inner boundary. We found that increasing the number of radial bins to over 1000 only led to changes in the planet migration times at the level of $\sim 10\%$. We hence chose 300 bins as acceptably accurate for a population synthesis study: many parameters of the model (such as viscosity parameter α) are known with a far worse precision anyway.

The disc is initialised with a surface density profile $\Sigma(R) \propto (1/R)(1 - \sqrt{R_{\text{in}}/R}) \exp(-R/R_{\text{disc}})$, where $R_{\text{disc}} = 100$ AU is the disc radial length scale, with the normalisation set by the total disc mass, M_d , integrated from R_{in} to R_{out} . The disc surface density is evolved by solving the time dependent viscous disc equation (cf. equation 1 in paper I), but now also including the disc photo-evaporation term to be explained below. The disc exchanges angular momentum with the planet via a prescription switching smoothly from type I into type II regime. The latter regime, when a gap in the disc is opened by the planet, is modelled by the widely used “impulse approximation” (e.g., Lin & Papaloizou 1986; Armitage & Bonnell 2002). The type I regime (no gap in the disc) is motivated by the results of Baruteau et al. (2011), parameterised via the planet migration timescale, t_I , given by

$$t_I = f_{\text{migr}} \frac{M_*^2}{M_p M_d} \frac{H^2}{a^2} \Omega_a^{-1}, \quad (1)$$

where a is the current position of the planet, $M_d = \pi \Sigma a^2$ is approximately the local disc mass, Ω_a is the local Keplerian angular velocity, and $f_{\text{migr}} \sim 1$ (see below) is a free parameter. The criterion introduced by Crida et al. (2006) is used to switch the planet migration between type I and type II. We emphasise that our approach conserves angular

momentum explicitly: the torque from the disc on the planet is equal to that of the planet on the disc with the minus sign, of course.

The disc viscosity is modelled as a Shakura & Sunyaev (1973) prescription, with the α viscosity parameter given by the sum of a constant term, $\alpha_0 = 0.005$ and a term that depends on the local self-gravity of the disc,

$$\alpha_{\text{sg}} = 0.2 \frac{Q_0^2}{Q_0^2 + Q^2}. \quad (2)$$

where Q is the local Toomre’s parameter. The parameter Q_0 , setting the transition from a viscosity driven by gravito-turbulence (e.g., Lodato & Rice 2005) to the non self-gravitating one, is set to $Q_0 = 5$ here. We found that lower values of Q_0 ($Q_0 = 2$ was used in paper II) result in the stars with discs fraction that is too high at early times, $t \lesssim 2$ Myrs. To fit observational constraints, one would either have to choose a much larger value of α_0 or require implausibly high photo-evaporation rates.

In paper II, disc photo-evaporation due to the host star’s UV and X-ray radiation was modelled as the sum of the fits to the respective photo-evaporation rates $\dot{\Sigma}_{\text{in}}(R)$ from Alexander & Armitage (2007) and Owen et al. (2012). The UV ionising photon luminosity of the star was set to $\Phi_{\text{ion}} = 10^{42}$ photons s^{-1} , while the X-ray flux of the star was $L_X = 2 \times 10^{30}$ erg s^{-1} . In this paper we employ the same approach, but also include the external photo-evaporation rate, $\dot{\Sigma}_{\text{ext}}$, by UV flux from nearby massive stars at 0.1 times the rates parametrised by Clarke (2007). This procedure in general is not guaranteed to satisfy observational constraints on disc dispersal, however. Following Mordasini et al. (2009a), we introduce a free parameter, $0 < \zeta_{\text{ev}}$, so that the photo-evaporation rate is given by

$$\dot{\Sigma}_{\text{ev}} = \zeta_{\text{ev}} (\dot{\Sigma}_{\text{in}} + \dot{\Sigma}_{\text{ext}}). \quad (3)$$

With this photo-evaporation prescription, the total photo-evaporation rate from the disc is equal to $\dot{M}_{\text{ev}} = 3.1 \zeta_{\text{ev}} \times 10^{-8} M_{\odot} \text{ yr}^{-1}$. As Mordasini et al. (2009a), we generate a uniform random distribution of $\log \zeta_{\text{ev}}$ bounded from below by ζ_{min} and ζ_{max} , and evolve a sample of ~ 1000 discs *without* planets. We then plot the fraction of stars with discs as a function of time, and compare it with the observationally established dependence, $\sim \exp(-t/t_{\text{ob}})$, where $t_{\text{ob}} = 3$ Myr (Haisch et al. 2001). By experimenting with values of ζ_{min} and ζ_{max} , it was found that a reasonably good agreement with the observations is obtained for $\zeta_{\text{min}} = 0.02$ and $\zeta_{\text{max}} = 10$ (cf. fig. 1). There is a certain degeneracy in this procedure. A higher value of disc viscosity (α_0) could be offset by reducing the photo-evaporation rate, but our main results do not depend on this level of detail.

2.2.2 Planet evolution module

The planet evolution module used in this paper is nearly identical to that described in section 4 of paper I. In brief, we model the pre-collapse gas fragment contraction using the “follow the adiabats” approach, which assumes the fragment to be strongly convective except for the boundary, and includes the radiative cooling of the fragment modified by the irradiation it receives from its surroundings (which can be very important, even unbinding the planet,

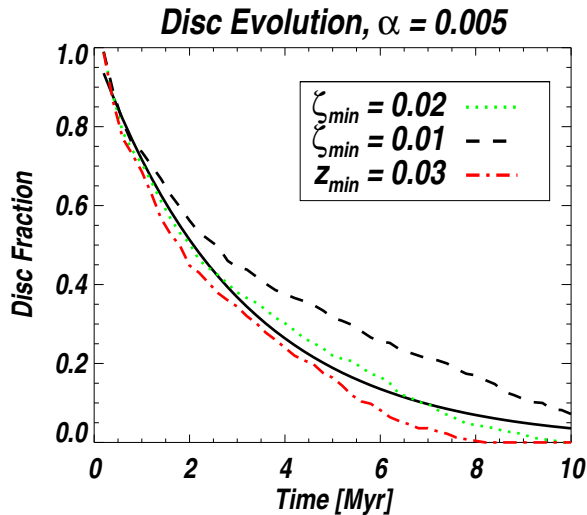


Figure 1. Fraction of stars with discs as a function of time for several values of the minimum disc evaporation factor ζ_{\min} , as labelled in the legend. The solid line gives the curve $\exp(-t/t_{ob})$, where $t_{ob} = 3$ Myr. $\zeta_{\min} = 0.02$ provides an acceptable fit to the solid curve.

see Cameron et al. 1982; Vazan & Helled 2012). The fragment is embedded in the disc if it migrates in the type I regime, and is hence bathed in the disc radiation with effective temperature of the disc mid plane. When the fragment migrates in type II regime, the irradiation from the central star and the edges of the gap carved by the fragment may be important. One difference from paper I is that we modify the intrinsic luminosity of the planet, L_{rad} , by introducing a “green house” effect for the planet immersed into the disc:

$$L_{\text{rad}} = \frac{L_{\text{iso}}}{1 + \tau_d}, \quad (4)$$

where L_{iso} is the luminosity of the fragment in isolation, and $\tau_d = \kappa \Sigma_a / 2$ is the disc optical depth at the planet’s location. This correction is necessary because the irradiation luminosity incident on the planet from the disc was calculated in paper I and II *neglecting* the planet’s energy input to the disc around the planet’s location. Furthermore, the disc thermodynamic properties are azimuthally averaged in our 1D approach, which additionally washes out the planet’s influence on the thermal balance of the disc in the planet’s vicinity ($\sim R_H$ or H , whichever is larger). The planet’s input into the disc temperature around its location must however be taken into account since massive planets (several Jupiter masses or more) can easily dominate the disc energy production around the planet (e.g., Nayakshin & Cha 2013). The planet’s luminosity calculated via equation 4 is therefore used in place of L_{iso} in equation (9) of paper I to determine the rate of planet’s radiative energy loss.

The dust physics used in this paper is identical to that described in sections 4.2, 4.3, and 4.6 of paper I. We use

three grain species – water, CHON¹ and rocks in relative abundances of 0.5, 0.25 and 0.25.

The total grain mass abundance is initially equal to the metallicity of the system, Z . The grains grow by sticking collisions, can sediment down modulo turbulence and convective grain mixing which oppose grain sedimentation. Grains can also be fragmented if they sediment at too high velocity, which in practice limits their size to a few cm at most. Grains vaporise once the given species vaporisation temperature is exceeded. Core assembly by grain sedimentation therefore depends sensitively on the temperature and convection of the inner regions of the gas fragment. The core growth prescriptions are identical to those presented in section 4.4 of paper I.

2.2.3 Atmospheres bound to solid cores

One significant modification to our treatment of the planet’s internal evolution is addition of an “atmosphere” around the growing massive cores. As found by Nayakshin et al. (2014), when the core reaches the mass of a few to a few tens of M_{\oplus} , the weight of the gas surrounding the core becomes comparable to the weight of the core itself. In Nayakshin et al. (2014), the structure of the core’s atmosphere was calculated assuming hydrostatic and thermal balance. Additionally, the outer boundary conditions for the atmospheric structure calculations were fixed by joining the atmosphere to a non-perturbed approximate analytical solution for a gas fragment from Nayakshin (2010a). Unpublished experiments done with a 1D radiation hydrodynamics code (described most recently in Nayakshin 2014, 2015a) showed that collapse of the atmosphere around the core does *not* actually lead to the collapse of the whole fragment, as assumed in Nayakshin et al. (2014). The physical reason for this is that during such a collapse contraction of the atmosphere generates a significant compressional energy, which is then communicated to the rest of the fragment by radiation and convection. The fragment then expands, which lowers the density at the fragment–atmosphere boundary. As the result, the core’s atmosphere’s outer layers also expand outwards, preventing further collapse of the gas layers near the core. This “feedback loop” prevents a hydrodynamical collapse of the whole fragment that was suggested to occur in Nayakshin et al. (2014). Physically, we expect a slow contraction of the atmosphere instead at the rate regulated by the cooling of the whole fragment.

To take this physics into account, we calculate the mass (and structure) of the atmosphere near the core at regular (short) time intervals. The atmosphere region is defined as that around the core where the total specific gas energy, $u - GM(r)/r < 0$, where u is the specific internal gas energy, r is the radius from the core, and $M(r)$ is the enclosed mass within that radius, including both gas and the core. If

¹ CHON is a mnemonic acronym for a material dominated by carbon, hydrogen, oxygen, and nitrogen, excluding water. Its composition, material properties and vapor pressure are here taken to be similar to that of the grains in the coma of Comet Halley Oberc (2004). CHON is a widely used component in planet formation theory (e.g., Pollack et al. 1996; Helled et al. 2008).

the fragment collapses due to H₂ dissociation then no modifications are done, since the atmosphere just becomes the part of the gaseous envelope of the planet. However, if the fragment is tidally disrupted, then the mass of the disruption remnant should be more massive than just the core (which was assumed in papers I and II). Specifically, if at disruption the mass of the atmosphere, M_{atm} , is lower than the critical mass for atmosphere collapse, $M_{\text{ac}} = (1/3)M_{\text{core}}$, then the mass of the survived planet is given by $M_p = M_{\text{core}} + M_{\text{atm}}$. However, if $M_{\text{atm}} > M_{\text{ac}}$, then we expect that a fraction of the total mass of the gas envelope would have accreted onto the core. Since our planet formation module is not yet sophisticated enough to calculate this fraction from first principles, we simply endow the core with gas mass randomly distributed in log between M_{ac} and the total mass of the fragment minus that of the core. This procedure is equivalent to a partial tidal disruption of a fragment, which typically results in planets with masses between a few tens of M_{\oplus} to ~ 1 Jupiter mass. We find that partial tidal disruptions of fragments more massive than $\sim 2 M_{\text{J}}$ are rare.

2.2.4 Monte Carlo initial conditions

Table 1 summarises the randomly drawn variables and their ranges used in this paper. The approach is similar to that from paper II: for each random variable, the distribution is uniform in the log of the parameter, and is distributed between the minimum and the maximum values given in Table 1. For example, the initial mass of the gas fragments is M_0 in Jupiter masses, with the log M_0 distributed randomly from $\log(1/3)$ to $\log 16$. Note that the logarithmic distribution for M_0 translates into the $dN/dM_0 \propto 1/M_0$ dependence for the mass function of the fragments, which corresponds well to the one observed for gas giants (Udry & Santos 2007, finds $dN/dM_0 \propto M_0^{-1.05}$). This range is far broader than the one used in paper II, where we only sampled the planets with initial masses in the range $0.5 M_{\text{J}} < M_0 < 2 M_{\text{J}}$. We hope to make tentative connections of TD hypothesis to the brown dwarf regime.

The disc mass is sampled between $0.075 M_{\odot}$ and $0.15 M_{\odot}$ of that. As explained in paper II, the mass of the disc at which the disc is gravitationally unstable (Toomre’s parameter $Q = 1.5$) is about $0.15 M_{\odot}$ (cf. fig. 1 in paper II) for the chosen initial surface density profile. Lower disc masses are considered here because 3D simulations show it is possible for fragments to be born in less massive non self-gravitating discs due to fragmentation induced by perturbations from fragments born at previous more massive disc epoch (e.g., Meru 2013). The fragments initial locations are sampled between 70 AU and 1.5 times that, which is reasonable since the minimum in the Toomre parameter is reached at $a \sim 90$ for our disc.

The opacity reduction factor is set to 1 in this paper (that is, the interstellar grain opacity of Zhu et al. 2009, not modified by grain growth, is used). The planet migration factor, f_{migr} , is sampled between 0.5 and 2, which is much smaller a range than the 1 to 10 range used in paper II. As in previous papers, we do not actually model the internal structure of the core, assuming it has a fixed density of 5 g cm^{-3} , and we hence cannot calculate the core’s luminosity self-consistently. To model the core’s luminosity, the Kelvin-Helmholtz contraction time of the solid core, t_{kh} , is

defined (see Nayakshin et al. 2014), and the core’s luminosity is prescribed as in section 4.4 of paper I. The parameter t_{kh} is varied between 10^5 and 10^7 years for the simulations in this paper.

The only exception from the uniform random parameter distribution procedure is the host star/disc metallicity distribution, which can be constrained observationally. It appears to be close to a Gaussian distribution in the CORALIE planet sample (Udry et al. 2000). As shown by Mordasini et al. (2009a), a good fit to the observations is provided by the Gaussian distribution

$$\frac{dp(Z_L)}{dZ_L} = \frac{1}{\sigma(2\pi)^{1/2}} \exp\left[-\frac{Z_L^2}{2\sigma^2}\right] \quad (5)$$

where $Z_L = [\text{Fe}/\text{H}] = [\text{M}/\text{H}]$, the usual logarithmically defined metallicity, $\sigma = 0.22$, and dp/dZ_L is the probability density. The subscript “L” on Z_L stands for “logarithmic”, since $Z_L \equiv \log_{10}(Z/Z_{\odot})$, where $Z_{\odot} = 0.015$ is the Solar metallicity (Lodders 2003), e.g., the fraction of mass in astrophysical metals compared to the total mass.

The metallicity distribution of the host stars used here is hence observationally motivated and differs from the fixed metallicity bins used in our previous papers. The metallicity of the disc and the initial metallicity of the planet, Z_0 are equal to that of the host star,

$$Z_0 = Z_{\odot} 10^{Z_L} . \quad (6)$$

3 RESULTS OVERVIEW

We performed 20,000 fragment-disc evolution experiments for this paper. In this section we provide an overview of the results, with further detailed analysis to follow.

3.1 The mass-separation plane

Figure 2 presents the population of planets produced by the end of our runs in the planet mass – separation plane. The mass of the planets is shown in the units of Jupiter masses on the left vertical axis, and in the Earth mass units on the right. To improve clarity of the figure, we reduce the number of planets (individual symbols) shown in the figure by randomly selecting a sub-sample of the planets. The regions to the left of the vertical dashed line (set at 0.1 AU) and below the horizontal dotted line (set at 0.05 M_{J}) show only 1/20th of the sample since these regions are very strongly crowded with planets. The remaining region – above the horizontal line and to the right of the vertical line – shows 1/2 of the sample.

The planets to the left of the vertical line are those that migrated through our inner boundary condition (operationally, they reached very close to it, $a = 0.09$ AU). Our choice of the inner disc radius, $R_{\text{in}} = 0.08$ AU, is somewhat arbitrary. It is likely that most of these planets will be driven so close to the star that they are either consumed by the star or are unbound by over-heating due to the intense radiation field of the star. However, we expect that magnetospheric interactions will cutoff the disc at different distances from the star in different systems. This cutoff distance will also vary with time in a given system as the accretion rate and

Table 1. The range of the Monte Carlo parameters of the population synthesis calculation. The first row gives parameter names, the next two their minimum and maximum values. The columns are: Planets initial mass, M_0 , in Jupiter masses; ζ_{ev} , the evaporation rate factor (cf. eq. 3); f_p , the pebble mass fraction determining the fraction of the disc grain mass in the pebbles; a_0 [AU], the initial position of the fragment; M_d , the initial mass of the disc, in units of M_\odot ; f_{migr} , the type I planet migration factor; t_{kh} , Million years, determines the luminosity of the core; α_d , turbulence parameter within the fragment; v_{br} , the grain breaking velocity, in m/s

Parameter	M_0	ζ_{ev}	f_p	a_0	M_d	f_{migr}	t_{kh}	α_d	v_{br}
Min	1/3	0.02	0.04	70	0.075	0.5	10^5	10^{-4}	5
Max	16	10.0	0.08	105	0.15	2	10^7	0.01	15

the magnetic field intensity vary. Due to these effects, we expect some of the planets that fell through our inner boundary to stop somewhere in the region between the star and R_{in} . For this reason we shall include a fraction of these planets in our further analysis and hence we show them in fig. 2. For these planets, the separation is a uniform random variable distributed between 0.03 AU to 0.09 AU.

The colours of the symbols are used to indicate the metallicity of the parent star as noted in the legend. For example, green symbols show the most metal poor stars, $[\text{M}/\text{H}] < -0.25$, whereas red show the most metal rich ones, $[\text{M}/\text{H}] > 0.25$. One can notice the prevalence of red over green for gas giant planets in the inner few AU, signifying the positive metallicity correlation reported in Nayakshin (2015b) and paper II. The outer tens of AU gas giants and the sub-Neptune planets below the horizontal line show much less, if any, metallicity preference, hinting on the absence of metallicity correlation there. These results were also found in paper II.

3.2 Statistics of fragment destruction and survival

We shall now look at the results in a different way. All 20,000 of our fragments are initially born at $70 < a < 105$ AU, yet there are just some hundreds of planets left in the region $a > 10$ AU by the end of the simulation. It is therefore clear from fig. 2 that most of the fragments migrate very close to the star, and are either disrupted and end up as low mass planets below the horizontal line, or migrate through the inner boundary of the disc and appear to the left of the vertical line.

For a more quantitative analysis of this, Figure 3 summarises the fate of our gas fragment migration experiments in two different ways. Fig. 3a shows the initial fragment and the final planet mass spectrum. The former is shown with the black histogram, and is uniform in mass from $M_{\text{min}0} = 1/3 M_J$ to $M_{\text{max}0} = 16 M_J$. The quantity shown in the histograms is $dN_p/dM_p \Delta M_p$, the number of planets found in the mass bin between M_p and $M_p + \Delta M_p$. Some deviations from a flat line in the figure are due to random Monte Carlo fluctuations in the fragment mass initialisation procedure, and also $M_{\text{min}0}$ and $M_{\text{max}0}$ falling inside the histogram bins rather than precisely on the bin edges.

The coloured histograms show the final masses of the planets after TD "processing" of the fragments in the disc. These are shown for all planets independently of where they end up in terms of their final planet-host separation. The populations are further broken on the metal rich bin, $[\text{M}/\text{H}] > 0$ (red colour), the metal poor bin, $[\text{M}/\text{H}] < 0$ (green) and the total (blue).

We see that the distribution of final planet masses

broadly divides into two groups: the disrupted one (fragments less massive than $1/3 M_J$ or $\sim 100 M_\oplus$) and those that avoided the disruption. The former population is more populous than the latter, as we shall see. The most populous group of disrupted planets are those that have masses from sub-Earth mass to $\sim 10 M_\oplus$. We notice that sub-Earth planets are more abundant in metal poor discs whereas super-Earths are more abundant at higher metallicities. This distribution however contains planets at all separations from the star and needs to be cut into more specific radial bins to learn more, which will be done below.

To digest the overall results of our simulations further, we find it useful to group the end outcome of the runs into:

- (i) Disrupted planets – those that were tidally disrupted anywhere in the disc between R_{in} and their birth position.
- (ii) "Assimilated" planets: those that migrated all the way to the inner boundary of our disc, R_{in} . Our calculations are oversimplified at the inner boundary, as pointed out above. In all likelihood, most of these fragments would be pushed closer to and possibly even into the star and thus be accreted (assimilated) by the star, although a minority may survive when the disc dissipates away.
- (iii) "Cold giants" – those fragments that survived tidal disruption and matured into a giant planet at large ($a > 10$ AU) separation from the star.
- (iv) "Warm giants" – those fragments that survived tidal disruption, and, despite the rapid inward migration, were able to stop outside the inner disc boundary but within $a < 10$ AU.

The frequency of these four outcomes are displayed in fig. 3b separately for the four metallicity bins. Note that tidal destruction of the fragments is the most common outcome ($\sim 80\%$ of the time) for Solar metallicity or less metal rich stars, but becomes progressively less common for the two metal rich bins, dropping to just over 20% for $[\text{M}/\text{H}] > 0.25$. This result is related to the positive metallicity correlation for gas giant planets found by Nayakshin (2015b) and in paper II: the higher the metallicity, the fewer giants are disrupted, and hence more giants survive per star.

Most of the fragments in the most metal-rich discs (red curve in fig. 3b) avoid tidal disruption. However, most of them end up migrating through the whole of the disc to R_{in} . As already suggested, a fraction of them is likely to survive inside R_{in} as "hot Jupiter". Focusing now on the population of gas fragments that were not tidally disrupted and not migrated through all of the disc (the last two entries on the horizontal axis in the figure), we observe that most of these reside at large separations from the star, $a > 10$ AU. The gas giant planets in the inner few AU is hence the rarest gas giant population in our synthetic models. Finally, it is pos-

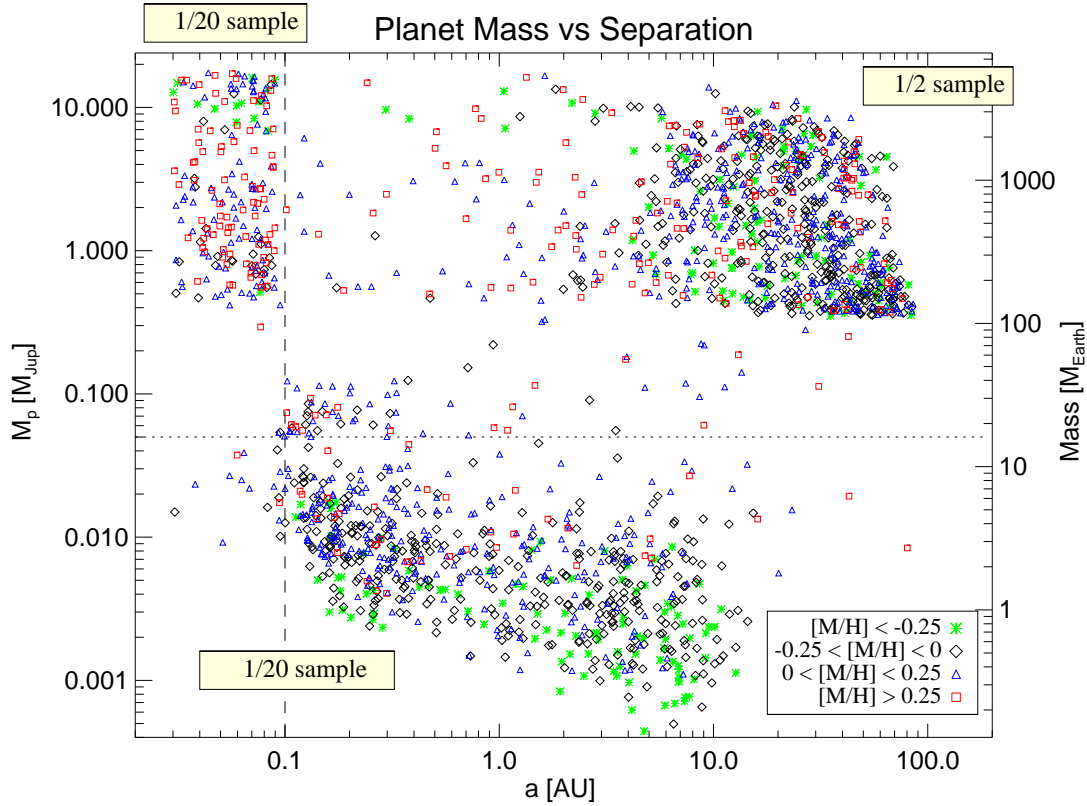


Figure 2. Simulated planets in the planet mass versus planet-host separation plane. The symbols and colours reflect the metallicity of the host stars, as detailed in the legend. For the sake of clarity, only 1/20th fraction of planets is shown to the left of the vertical line and also below the horizontal line. 1/2 of all planets is shown in the right top quartile of the plane.

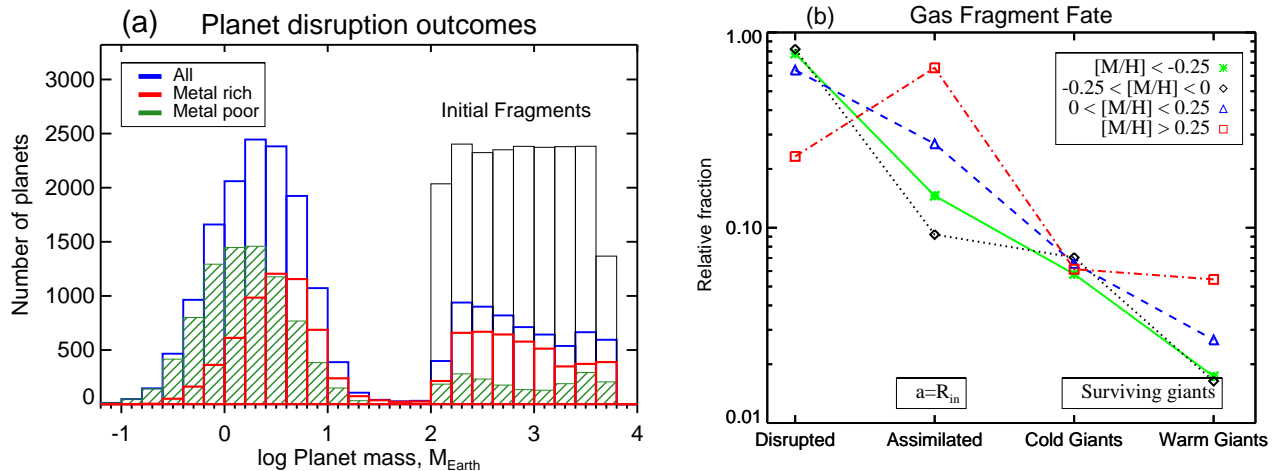


Figure 3. (a) Comparison of the initial mass spectrum of fragments (black diagram) to the final distribution of planetary masses. The colours group the results by metallicity, with low metallicities defined as $[M/H] < 0$ and high defined as $[M/H] > 0$. (b) The outcome of gas fragment migration experiments in terms of the fraction of the initial fragments that are tidally disrupted, pushed all the way into the star ("assimilated"), survive as gas giant planets at all separations, or survive as "warm giants" here defined as planets at separations less than 10 AU.

sible to notice a strong positive correlation with metallicity in the fraction of giants survived in the inner disc ("warm giants") and no such correlation in the outer disc.

4 HOT PLANET MASS FUNCTION

The planet mass function (PMF) is one of the most interesting observables of a planet population. Figure 3a presented the mass function of planets formed in our simulations at all separations. The observed PMF are available only for close-in planets at this point in time as directly imaged planets are rare (e.g., Bowler et al. 2015) and can only sample planets more massive than $\sim 1 M_J$. We shall therefore focus our attention on the inner part of the mass-separation diagram.

Since our model is still in the development stage, we shall not attempt a detailed comparison between the theory and the data by performing a synthetic "observation" (see Mordasini et al. 2009b) of our planets. Instead, we shall make a rather crude cut of the parameter space by carving out a "hot" planet sample which we define as the planets found within the inner 5 AU of the host star plus a 10% fraction of the "assimilated" planet group, that is, those planets that ended up at $a = R_{\text{in}}$. The latter group of planets is included in our analysis for the reasons explained in §3.1 which is also similar to the approach of Mordasini et al. (2009b). Specifically, our inner boundary condition is too simple at this stage of the model development, yet observations, especially transit surveys, are heavily biased towards these planets. We expect that some of the simulated planets at $a = R_{\text{in}}$ will survive in the region between the star and $a = R_{\text{in}}$. Our 10% choice of planets at $a = R_{\text{in}}$ is ad hoc but this choice does not influence any of the conclusions of this paper significantly. We also consider below a planet sample that does not include the assimilated planets at all.

4.1 Massive planets

The top panel of fig. 4 shows the PMF of the hot planet sample for planets with mass greater than $10 M_{\oplus}$. We show two versions of PMF. The histogram shown with the blue line shows all the planets in the sample. The shaded red color histogram shows the same sample but with a rudimentary RV-selection criterium of the stellar Doppler shift velocity exceeding $v_{\text{det}} = 3$ m/sec. To enable this selection, we generate a random uniform distribution of $\cos i$, where i is the inclination angle of the planet's orbit ($i = 0$ corresponds to viewing the star-planet system along the rotation axis). The stellar Doppler's velocity as seen by the observer is then

$$v_* \approx v_K \frac{M_p}{M_*} \sin i, \quad (7)$$

where $v_K = \sqrt{GM_*/a}$ is the planet's circular Keplerian velocity at its position, a , and $M_* = 1 M_{\odot}$. We then prescribe the probability of detecting a planet with a given v_* value as

$$P_{\text{det}}(v_*) = \frac{v_*^2}{v_*^2 + v_{\text{det}}^2}. \quad (8)$$

This is ad-hoc, but is asymptotically correct, so that all the planets with large $v_* \gg v_{\text{det}}$ are detected, whereas none of the planets with $v_* \ll v_{\text{det}}$ are detected. The smooth

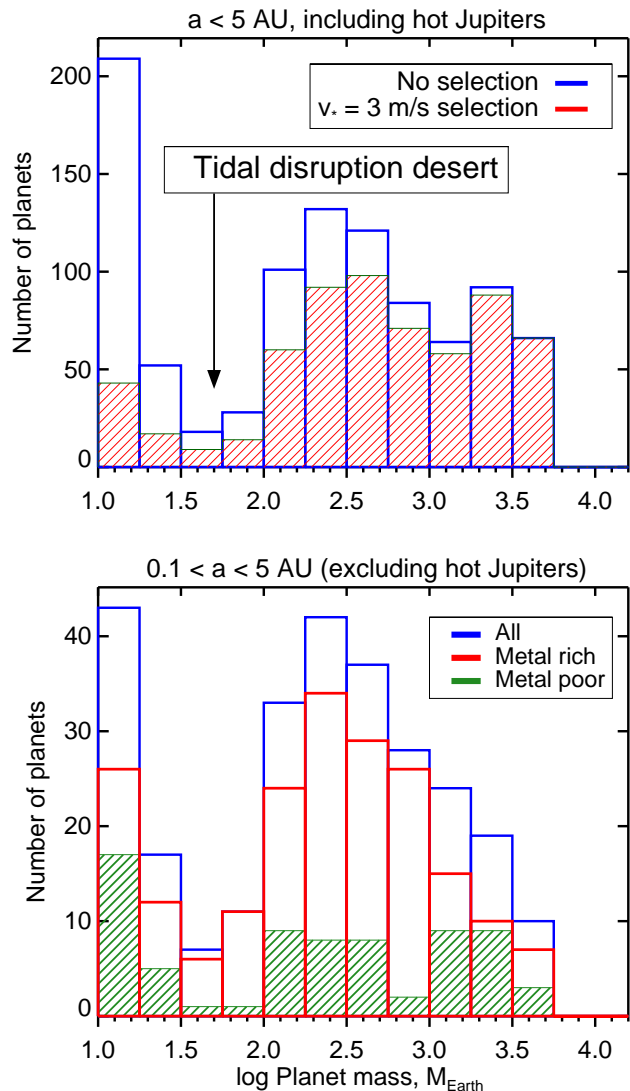


Figure 4. Planet mass function (PMF) from simulations. The top panel is the "hot planet sample" defined in §4, with 10% of "hot Jupiter" planets included. The blue shows all planets whereas the red histogram shows planets affected by a velocity cut. The bottom panel shows planets in the same spatial disc region, with velocity cut imposed, but now excluding planets at $a < 0.1$ AU. The colours on the bottom panel separate metal rich and metal poor host populations. See §4.1 for detail.

transition is more realistic than applying a sharp cutoff by requiring detection only for planets $v_* > v_{\text{det}}$. The mass shown in the histogram selected by $v_* > v_{\text{det}}$ m/s is $M_p \sin i$ rather than M_p , of course.

The bottom panel of fig. 4 shows the PMF of the simulated planets, with the velocity cut applied, and in which no planets inside the inner disc edge were included, so that $a \geq 0.1$ AU for all of these planets. We also separated the population on the metal rich (red) and metal poor (green) samples.

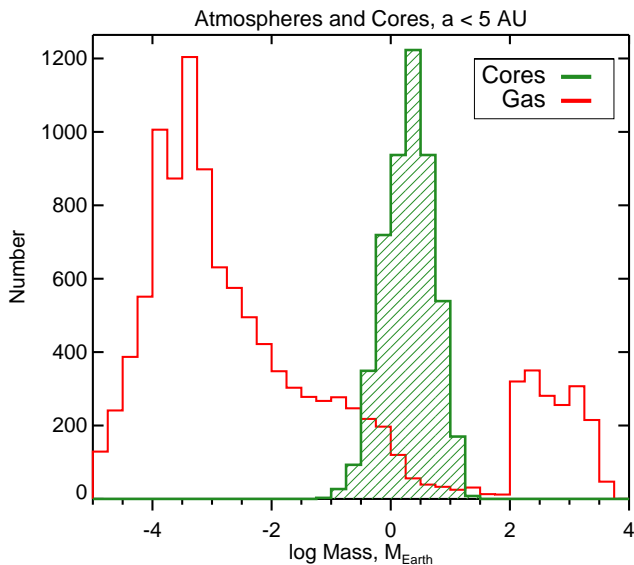


Figure 5. Mass function of bound gas in the simulations (red histogram), compared with that of the cores (shaded green). The latter is scaled down by a factor of 3 for clarity. The bound gas is either self-bound (the high mass peak to the right) or is attached to numerous low mass cores (low mass part of the red histogram), with little in between.

4.1.1 Tidal disruption desert

One of the notable features of the simulated PMF, in both projections in fig. 4, is the deep depression in the number of planets with masses between $\sim 20 M_{\oplus}$ and $\sim 100 M_{\oplus}$. An appropriate name for the feature is “Tidal Disruption desert” as it is due to the following. To the right of it, there are massive $M_p \gtrsim$ a few hundred M_{\oplus} gas-dominated planets that did *not* experience a tidal disruption. To the left, on the other hand, are much smaller rocky core dominated planets that are the most abundant remnants of the disruptions. The planets inside the desert, on the other hand, are the planets that went through a partial disruption. These planets consist of a massive solid core dressed in a very dense gas envelope bound to the core as explained in section 2.2.3. The gas masses of these envelopes are comparable to or a few times larger than their core masses. We find that such planets are rare for the simulations presented in this paper.

To expand on this point, fig. 5 compares the mass function of all gaseous envelopes at $R_{\text{in}} < a < 5$ AU, shown in red colour, with that of the cores (shaded green histogram). We see that gas envelopes (which may be quite metal rich, see §6) display a certain bimodality: they are either very low mass or very high mass. The low mass atmospheres are the majority; these are envelopes bound to low mass cores ($M_{\text{core}} \lesssim$ a few M_{\oplus}). Higher mass cores attract more massive atmospheres, but then the number of massive ($M_{\text{core}} \gtrsim 10 M_{\oplus}$) cores is small, and hence the number of more massive gas envelopes plunges as well. At gas mass of about $100 M_{\oplus} \approx M_{\text{min}}$ and above there is the domain of the undisrupted gas giants.

While we are very confident that the Tidal Disruption desert is a robust feature of our model, its depth is probably

not modelled reliably enough yet. The bound atmosphere structure is dependent (Nayakshin et al. 2014) on the poorly known opacity and the equation of state (Stamenković et al. 2012) of massive cores that are much hotter than present day cores of gas giant planets are believed to be. Additionally, our equation of state for the gas in the region very close to the core (see Hori & Ikoma 2011, for how this may affect the critical core mass) is over-simplified. Formation of more massive atmospheres than found here would fill the desert somewhat, although evaporation of atmospheres very close to the star (e.g., Owen & Wu 2013), not modelled here, could empty it further.

Note that Core Accretion model also predicts a “planet desert” at a similar planet mass (Ida & Lin 2004b; Mordasini et al. 2009b), for a seemingly different but actually nearly identical physical reason. In CA, $M_{\text{core}} \sim 10 M_{\oplus}$ is the critical core mass at which point a runaway accretion of gas onto the planet commences. Planets growing in the disc “travel” through the desert quickly to reach the higher mass ($M_p \sim 1 M_J$) peak, so that the chance of a planet stranded inside the desert is relatively low.

The lesson from this is that the structure of the planets may not always (or perhaps even rarely?) be used to constrain the formation route of a planet (see also Helled et al. 2013). In the case of the desert in the PMF, atmospheres with masses $\sim M_{\text{core}}$ are unlikely, whether the planet is built bottom-up as in CA or top-down as in the TD. This is more of a fundamental property of matter than a consequence of a particular formation mechanism. It therefore appears that some other observational diagnostic must be used to distinguish between CA and TD models. Metallicity correlations, dependences of the PMF on the mass of the host star, or timing of planet formation may hopefully break the degeneracy in the future.

The observed planet mass function also shows a strong depression above $\sim 20 M_{\oplus}$ Mayor et al. (2011); Howard et al. (2012) but it does not have the bump at ~ 1 Jupiter masses that both our and CA models predict. We shall study this issue further in the future, but for now we note that a more efficient destruction of gas giant planets than our current calculations would reduce their number in fig. 4, and also increase the number of planets in the “desert region”, making the models more compatible with observations.

4.1.2 Over-abundance of very massive planets

Another feature of the theoretical PMF shown in the top panel of fig. 4 is that the number of very massive planets, $M_p \gtrsim 10 M_J \approx 3200 M_{\oplus}$, is too large compared with the observed PMF. This region in the PMF is however sensitive to the initial fragment mass function shape, which we set to $dN_f/dM_f \propto 1/M_f$ (cf. fig. 3a). This would yield a flat PMF histogram. The distribution of initial fragment masses is not well constrained theoretically, and it may well be steeper than the one we used here.

Furthermore, we also made the simplifying assumption (iv) in §2.1 that fragments do not accrete gas. It is possible that the most massive fragments do accrete gas rapidly (cf. simulations of Nayakshin & Cha 2013; Stamatellos & Herczeg 2015), so that they “run away” into the regime of low mass stellar companions

(Stamatellos & Whitworth 2008), which would remove them from our theoretical PMF.

To expand on this, we note that the maximum available mass budget of gas to be accreted on a fragment is the mass of the disc, which is $0.15 M_{\odot}$ (see Table 1) for the simulations presented here. However, this is a limitation of our set-up rather than a physical one. We here investigate only one fragment per disc, which makes most sense when the disc self-gravity is in its dying phase, and hence the disc mass is moderate. Real systems may however form gas fragments earlier on, in class 0 stage, when the protostar is only a fraction of its central mass, and when the disc is still being fed from the protostar’s natal molecular envelope. If there is a “runaway” accretion for more massive gas fragments as discussed in Nayakshin & Cha (2013), then these fragments may grow to massive BDs and even low mass stellar companions. There is hence a potential connection of TD theory to low mass stellar companions, which may be another way to test it. This is however just a speculation in this point; gas accretion onto the fragments must be included in the calculations properly for reliable theoretical predictions.

4.2 Core-dominated planets

We now focus on core-dominated planets. We select the planets less massive than $M_p < 10^{1.5} M_{\oplus}$, slice the resulting subsample into three spatial bins, and plot their PMF in figure 6. The histogram in blue shows the population of cores closest to the host star, in $a < 0.5$ AU region. The red histogram covers the region $0.5 < a < 5$ AU, and the green histogram shows cores located further out.

4.2.1 No pool of close-in very low mass cores

Fig. 6 shows that the inner 0.5 AU region contains very few cores less massive than $1 M_{\oplus}$. The absence of sub-Earths is due to the fact that tidal disruptions producing such low mass cores typically occur further out, at a few to 10 AU region. The low mass cores migrate slowly since the migration rate is proportional to the core’s mass, cf. eq. 1. Most of them therefore do not make it inside the inner 0.5 AU region.

This result will probably be weakened to some degree by more realistic calculations that would include previous generations of fragments during earlier disc phases. Cores located in the inner few AU may get locked into resonances (e.g., Paardekooper et al. 2013) with gas fragments migrating from the outer disc and hence be pushed inward along with the fragment more rapidly than they could migrate by themselves. If the fragment is then tidally disrupted and the gas is consumed by the star, a second low-mass rocky core will be left behind. If observed at the present time, the system would have no obvious record of a past outer massive fragment’s existence. Additionally, once the gas disc is removed, the N-body interactions of cores with each other may bring more low mass cores into the innermost region.

Despite this, the rollover of the core mass function at low masses is a general result of our model for all separations

(cf. fig. 6), although the core mass at which the rollover occurs decreases with increasing separation. Therefore, while the exact core mass at the rollover is subject to further modelling, its existence is a robust result.

We emphasise the difference from the Core Accretion way of building cores here. In CA, *all* of the solid mass is initially in tiny bodies (planetesimals). In the early stages of planetary growth, most of the mass is in the low mass cores and “embryos” with mass well below $1 M_{\oplus}$. The PMF from CA calculations thus shows a strong peak at low masses, $M \lesssim 1 M_{\oplus}$, see fig. 3 in Mordasini et al. (2009b) and fig. 2 in Mordasini et al. (2012). There is no physical reason to have such a divergence towards smaller masses in TD theory for planet formation since the cores grow by accretion of grains and not by collisions of numerous solid “embryos”.

We note that this prediction of the model is consistent with *Kepler* observations (Howard et al. 2012) that find that the frequency of planet occurrence (corrected for observational biases) does not diverge and instead drops towards the smallest radius planets ($R_p \sim R_{\oplus}$).

4.2.2 A smooth PMF with no local minima at a few M_{\oplus}

Another interesting distinction between our calculations and that of CA theory is that some of the latter predict that the cores can be composed of two separate populations – the inner smaller rocky cores and the outer more massive icy cores. Some of CA models (e.g., see figs. 8 and 13 in Mordasini et al. (2009a) and fig. 3 in Mordasini et al. (2009b)) show a significant dip in the PMF in-between these two populations, at $M_{\text{core}} \sim$ a few M_{\oplus} . The fact that the low mass cores are rocky and the high mass ones are icy is best seen in figures (especially 5, 7 and 11) in Alibert et al. (2013).

As will be seen later, our cores, including the most massive ones, are rock-dominated, and therefore there is no physical reason for two separate populations to exist in the PMF of the cores. It is hence a smooth function of M_{core} (fig. 6).

4.2.3 A rollover above $\sim 10 M_{\oplus}$

The population of cores shown in fig. 6 in the inner 0.5 AU is dominated by super Earths of mass $\sim 5 M_{\oplus}$. There are very few cores more massive than $10 M_{\oplus}$. As noted in §2.2.2, in TD cores grow by grain sedimentation, and this process is limited by the rate at which the grains can sediment without fragmenting in high speed collisions, and also by the convective mixing of the grains which tends to bring the grains from the centre back into the outer regions of the fragment (cf. paper I and also Helled & Bodenheimer (2010)). Massive cores are very luminous in our model. This amplifies convection in the inner parts of the fragment, forming a kind of a feedback loop that limits the rate at which the cores grow.

Therefore, the absence of more massive cores in our models appears to be due to an insufficient time during which the conditions within the fragments are conducive for core growth. For a rapid core growth, the fragment must be (a) dense enough to allow an efficient grain growth and sedimentation, (b) but not too hot for the grains to vaporise and for the fragment to collapse into the second core

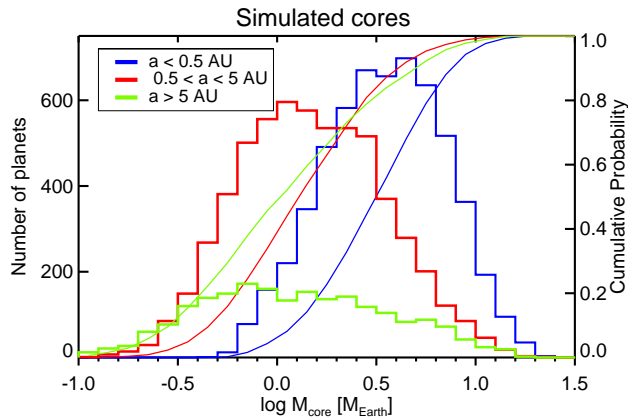


Figure 6. Planet mass function (PMF) of cores from simulations in three different spatial regions as explained in the legend. The vertical scale on the right shows the cumulative probability distribution for the same curves. See §4.2 for detail.

when the core will be buried under all the weight of the gas. The core growth time window is also limited by the lifetime of the fragment from its birth to the moment it is tidally disrupted.

The precise value of the upper rollover mass in the core-dominated part of the PMF does depend on parameters of the models and the atmosphere presence for the most massive cores. To explore this issue, we slice the sample of planets for $a < 0.5$ AU into two sub-population for which the grain breaking velocity, v_{br} , is between $5 < v_{br} < 7$ m s $^{-1}$ and $12 < v_{br} < 15$ m s $^{-1}$, and plot the resulting mass function in fig. 7. The higher breaking velocity sub-population naturally has more massive cores because the grains can sediment at higher velocity. This shows that the exact shape of the mass function near $M_p \sim 10 - 30 M_{\oplus}$ is not well constrained at the moment. Additionally, it is possible that accretion of gas or pebbles after the tidal disruption of the fragment would increase the mass of the planets shown in fig. 6 somewhat.

The red histogram in fig. 6 shows that low mass planets (mainly bare cores) become more dominant at larger separations. This is due to the fact that high mass cores migrate inward much more than do low mass cores. The green histogram indicates that there are relatively few cores beyond 5 AU. This result is however sensitive to the migration prescription and the speed with which the most massive cores are assembled; fig. 4 in paper II shows a much larger population of cores formed at tens of AU from the host star.

5 PLANET METALLICITY PREFERENCES

We shall now analyse how the host star metallicity influences the likelihood of planet formation of different types. To reiterate the setup described in §2.2.4, our metallicity distribution is a Gaussian (equation 5) with the mean $[\text{Fe}/\text{H}] = [\text{M}/\text{H}]$ equal to zero and the dispersion around that $\sigma = 0.22$, motivated by the CORALIE planet sample. The nature of the resulting dependences turn out to vary from a region to a region in the planet’s mass-separation plane; thus we shall study these regions separately.

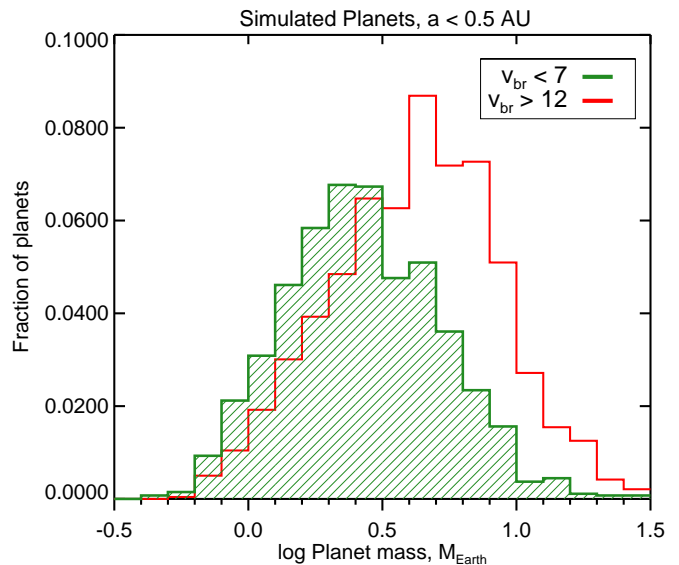


Figure 7. Mass function of low mass planets in the inner 0.5 AU for low and high grain breaking velocities, as specified in the legend (v_{br} is in units of m/s). Unsurprisingly, more massive cores are assembled within the fragments if grains can sediment without fragmenting at higher velocities.

5.1 Moderately massive giants vs super Earths in the inner 5 AU

We now analyse the metallicity correlations in the hot planet sample (see §4.1: the planets found within the inner 5 AU of the host star plus a 10% fraction of the ”assimilated” planet group, that is, those planets that ended up at $a = R_{in}$). From this sample we then select super Earths defined as planets in the mass range $2 M_{\oplus} < M_p < 15 M_{\oplus}$, and moderately massive giants as gas giants with mass between at least $100 M_{\oplus} \approx 0.3 M_J$ and $5 M_J$. More massive giants are rare in the observed samples. There is also a physical reason to look at the metallicity correlations of the more massive giants separately, as we will see in §5.3.

Fig. 8 shows how these two groups of planets are distributed over the host star metallicities. The blue line histogram shows the giants, whereas the red histogram shows the super Earths. The curves of the same colour show the respective cumulative distributions with the scale on the right vertical axis. If our theory were insensitive to the metallicity of the host star, then we would expect to see a Gaussian-like distributions centred on zero in fig. 8. However, it is evident that gas giants appear preferentially around metal-rich hosts, whereas super Earths are spread about the mean metallicity roughly symmetrically. Also note that the frequency of finding a gas giant *per star of a given metallicity* keeps increasing with $[\text{M}/\text{H}]$ up to the highest value of 0.5 shown in the figure (see fig. 10 below). The reason why the gas giant histogram goes down in fig. 8 is that there are very few stars with metallicities larger than $[\text{M}/\text{H}] = 0.3$.

As explained in Nayakshin (2015b) and papers I and II, the positive metallicity correlation for giants is due to pebble accretion rate onto the fragment being larger at higher metallicities, which leads to the fragment contracting faster.

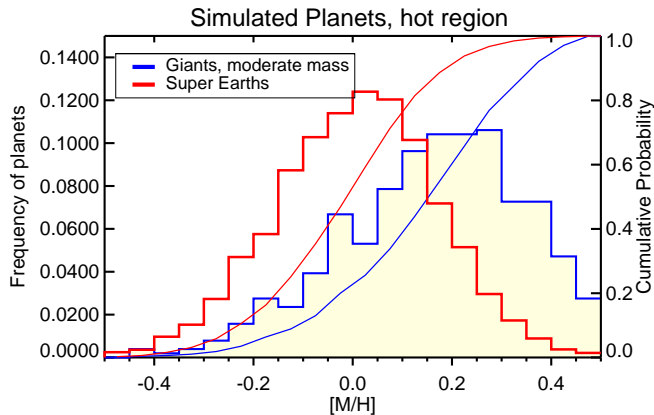


Figure 8. The fractional distribution of gas giant planets (blue filled-in histogram) and super Earths (red histogram) over metallicities of the host stars. Only planets in the inner 5 AU are selected. The curves of the respective colours show the cumulative distributions of same planet groups. Note strong positive metallicity correlation for gas giants and absence of such for super Earths. See text in §5.1 for more detail.

Faster contraction implies fewer tidal disruptions, and hence more gas giants surviving at higher metallicities. The physical reason for pebble accretion being so influential in controlling the rate of the fragment’s contraction is that pebbles bring in additional mass into the fragment (but not kinetic energy since they sediment onto the cloud gently or else they break up in high speed collisions). Gas clumps dominated by molecular hydrogen turn out to be very sensitive to addition of mass in this way and collapse when the mass of the extra metals reaches $\sim 5\%$ to $\sim 20\%$ of the initial fragment mass. This picture also has implications for metal overabundance in giant planets as a function of their mass as we shall see in §8. The more massive the fragment is, the hotter it is at birth, the less pebbles is required to bring it to the H_2 dissociation instability point (when the central fragment’s temperature is ≈ 2000 K).

The metallicity correlation for super Earths turns out to be a much subtler matter. Fig. 8 shows that high metallicity environments are no more preferable for formation of cores in the mass range $2 M_{\oplus} < M_p < 15 M_{\oplus}$ than low metallicity discs. In paper II, two explanations for this result, both working in the same direction, were proposed: (a) saturation in the mass of the most massive cores within the fragment at high metallicities, and (b) disruption of high metallicity gas fragments being too rare. The latter effect is important because super Earths are the remnants of these disruptions: no disruptions, no super-Earths.

We now investigate the relative importance of these two effects. The top panel of Fig. 9 shows the mass function of cores found in our simulation in the inner 5 AU for four metallicity bins as specified in the legend. This panel shows that most of the super Earths form at metallicity not too dissimilar from the Solar metallicity (the blue and the green histograms). The curves are normalised by the total integral giving the total number of cores, of course. The bottom panel of the figure shows the distribution of frequency of planet masses for the curves in the top panel; the histograms on the bottom are normalised on unity for each metallicity bin. It is clear from the bottom panel of fig. 9 that the mean mass

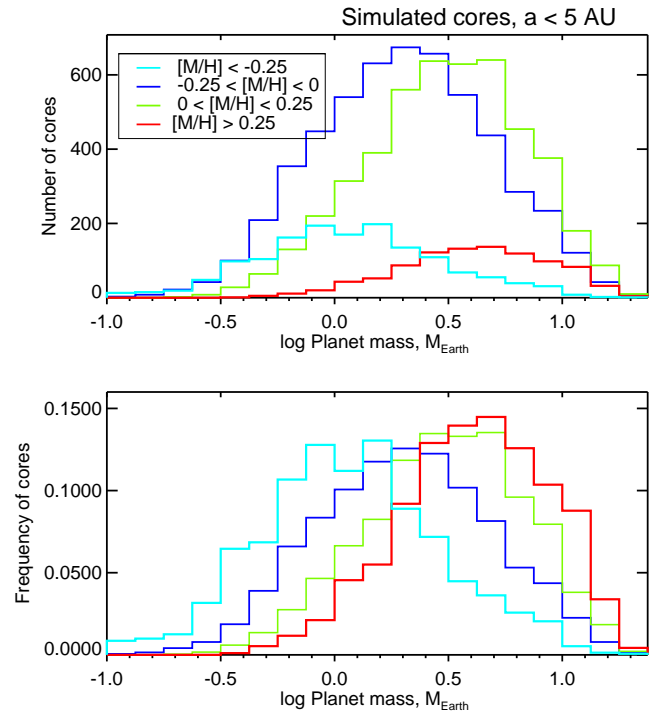


Figure 9. Number (top panel) and fractional (lower panel) mass distributions for cores found in the inner 5 AU for four different metallicity groups.

of the core increases with metallicity rapidly while $[M/H] < 0.25$. However, the mean core mass increases less between the two metal rich bins. There is thus indeed a certain saturation in the cores mass growth at high metallicities, although the mean core mass still increases with $[M/H]$. Thus effect (a) is not actually that strong.

The main driver of the poor correlation between super Earths and host’s metallicity in our models turns out to be (b), e.g., that the number of tidal disruptions is just too low at high $[M/H]$, yielding too few cores (although on average they are more massive than the cores at lower metallicities). Figure 10 shows the frequency of the fragment becoming a given planet type as shown in the legend versus metallicity of the host star. In particular, the black connected diamonds show the frequency of obtaining a super Earth in the inner disc. The red crosses show the frequency of the fragment migrating through all of the disc to $r = R_{in}$ without being disrupted. Notice the anti-correlation between such undisturbed fragments and the number of super Earths. In particular, at the highest metallicities, as much as $\sim 70 - 80\%$ of our initial fragments manage to collapse and migrate all the way in, avoiding tidal disruption. This of course must mean that fewer core-dominated planets are made in this environment because there are fewer tidal disruptions.

Summarising these findings, we conclude that Super-Earths do not correlate with metal abundance of host star in our models *because gas giant planets do*. The presence of a gas giant planet indicates that its predecessor, a pre-collapse molecular fragment, was successful in avoiding the tidal disruption. Since gas giants are most frequent at high metallicities, gas fragment disruptions must be much less ubiquitous at high $[M/H]$, and hence there should be fewer Super-

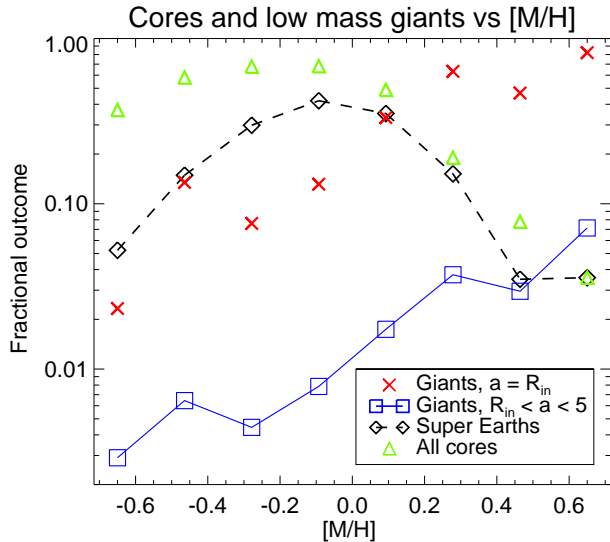


Figure 10. Frequency of a fragment becoming a planet of a given type, as shown in the legend, as a function of the host star metallicity. Note that at the highest metallicity bins, most fragments are able to migrate to $a = R_{\text{in}}$ and hence only a few super Earths are made. Also note that it is the blue square line that should be compared with Fischer & Valenti (2005), since this line shows the frequency of finding a gas giant per star of a given metallicity, rather than that in the stellar population as a whole, which is presented in fig. 8.

Earths. On the other hand, we note that the mean mass of the cores does increase with metallicity. Thus, Super-Earths made by TD model may be said to correlate in mass (somewhat weakly at high core masses) but not in numbers with the metallicity of the host star.

The histogram distribution for our simulated planets shown in fig. 8 looks quantitatively similar to fig. 2 in Buchhave et al. (2012), even though we did not make any attempt to arrive at such an agreement specifically.

5.2 Cold giants are metal insensitive

We now compare the metallicity correlation for all of the gas giant planets $M_p > 100 M_{\oplus}$ in the hot sample of §4.1 with the same mass range planets located further out, at $R > 10$ AU, which we name “cold giants”.

Figure 11 compares the metallicity distributions of the hot and cold giants. As was the case with Super-Earths discussed in §5.1, the cold giants show little metallicity preference. The mean of the hot giant distribution is at $[M/H] = 0.12$, clearly showing a significant positive metallicity preference, whereas for the cold giants we find $\text{mean}[M/H] = -0.01$.

The interpretation of this result is straightforward. Most of the fragments that stayed behind 10 AU did not come close enough to the parent star to experience tidal forces sufficiently strong to rip the fragments apart. Therefore, these planets survive irrespectively of how much pebbles was accreted. They are therefore insensitive to the metal content of the parent discs.

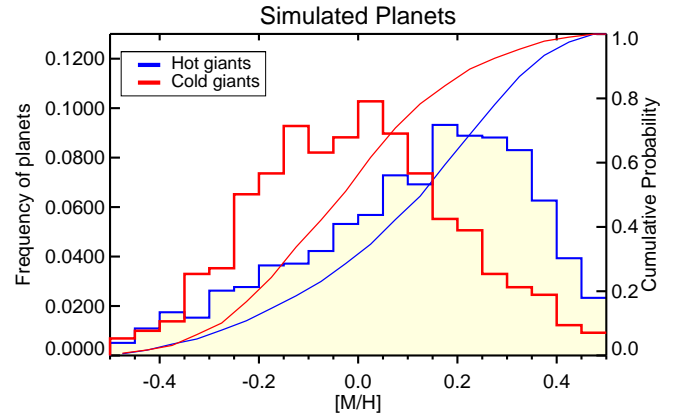


Figure 11. Same as fig. 8 but now comparing the metallicity distribution of gas giant planets in the inner 5 AU (hot giants) with those in the “cold” region, $a > 10$ AU (red histogram). Note that cold giants show no metallicity preference.

5.3 Most massive giants are metal insensitive

Finally, we come to the most massive planets studied in this paper. A visual inspection of the top left hand corner of Figure 2 shows that metal poor massive giants ($M_p \sim 10 M_J$) are about as abundant as metal rich planets of same mass. This appears true for planets at the inner disc edge and also in the inner few AU, so it may be general for the whole sample of the most massive planets.

Figure 12 shows that this is indeed the case. Similar to fig. 10, this figure shows how frequency of an initial fragment becoming a given type of planet changes with the host star metallicity. Three groups of gas giants is considered in fig. 12. The fraction of survived moderately massive giants (the blue diamonds curve) is a rapidly increasing function (roughly a power law $\propto Z^{5/4}$, where $Z = Z_{\odot} 10^{[M/H]}$), reflecting the strong positive correlation for the hot moderately massive giants discussed in §5.1.

The black squares curve in fig. 12 shows the survival fraction for more massive giants, $M_p > 5 M_J$. We see that the probability of these massive fragments surviving the disc migration phase inside the hot region is actually flat with metallicity. Further to that, the red crosses show the fraction of the initial fragments in the massive sample that migrated all the way to the innermost disc radius. The curve has a depression at metallicities just below the Solar value, which is to say that fragments around stars of nearly Solar composition are the most likely to be tidally disrupted before they arrive at $a = R_{\text{in}}$.

For the most massive fragments, therefore, very high or very low metallicity environments are actually preferable (although not by much, e.g., less than by a factor of 2). This bimodality of metallicity preferences of high mass giants forming in the context of TD was hinted on in Nayakshin (2015a), where it was shown that gas giant planets contract and collapse in one of two ways. The most well known way, studied in literature on giant planet evolution since Bodenheimer (1974); Bodenheimer et al. (1980), is by radiative cooling, when the planet radiates its excess thermal energy away before collapsing. The second way is by metal loading via pebble accretion, in which case it is the increasing weight that leads the planet to collapse. The radiative cooling time of the

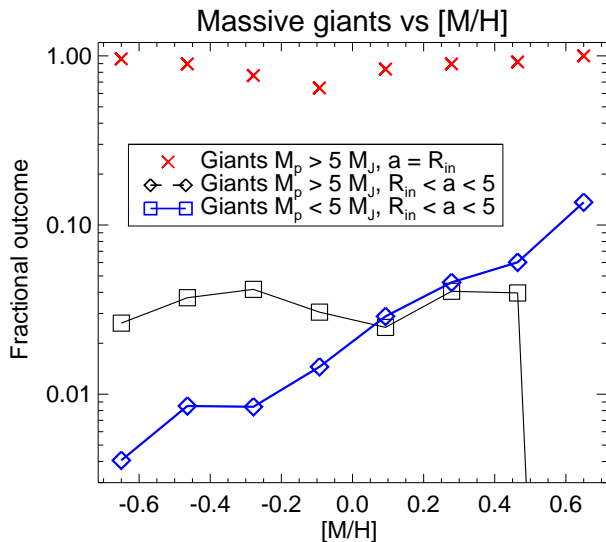


Figure 12. Similar to fig. 10: frequency of the initial fragments becoming a planet in the three mass-separation ranges defined in the legend. Note that low to moderate mass giants (blue line) correlate positively with metallicity, whereas high mass giants do not.

fragments is a strongly decreasing function of the fragment’s mass (cf fig. 1 in Nayakshin 2015a). In section 7 of that paper, it was suggested that even at large grain opacities, that is not modified by grain growth, high mass fragments are capable of contracting faster by radiative cooling than by pebble accretion.

The radiative cooling rate of the fragment decreases with grain opacity, which is directly proportional in our model to the total mass of metals in the planet minus the mass of the core. Therefore, at higher metallicities the radiative cooling channel for collapse of massive fragments is no longer efficient. However, pebble accretion does help at the highest metallicities, explaining why the curve shown with the red crosses recovers to almost unity at high $[M/H]$.

Summarising this discussion, the metallicity correlation for the highest mass giant planets is essentially a sum of two correlations: (i) an anti-correlation for the radiatively cooling fragments predicted by Helled & Bodenheimer (2011) and (ii) the positive correlation due to pebble accretion (Nayakshin 2015a). The reason why the anti-correlation becomes important only for high mass $M_p \gtrsim 5 M_J$ planets and not lower mass planets is that for lower mass planets the radiative cooling channel is not important at all compared with the pebble accretion, even at very low metallicities.

One caveat must be emphasised here. We do not include accretion of gas onto pre- or post-collapse giant planets (see point (iv) in §2.1). It is conceivable that some of the observed massive $M_p \gtrsim 5 M_J$ planets could have started from gas fragments of lower mass (even in the context of TD). If this is the case then those planets would correlate with metallicity positively since their progenitor fragments did. This would dilute the effects we discussed here, but we are not yet able to quantify by how much.

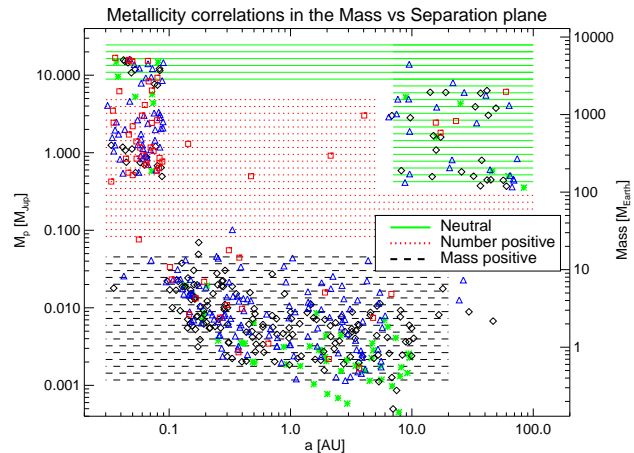


Figure 13. The planet mass versus host separation plane, with 1/40th of the simulated planets shown, shaded by the type of metallicity correlation in the respective region. “Number positive” and “Mass positive” are correlations in which the frequency of planets or the only the mass of the planet correlates with the star’s metallicity, respectively. See text in §5.4 for explanation. The symbol colour meanings are same as in fig. 2.

5.4 Metallicity preferences, simulation vs data

In the previous sections we presented theoretical predictions on how planets correlate with the host star’s metallicity in a number of regions in the planet mass – host star separation plane. For convenience, these are summarised graphically in fig. 13 in which we show a small subset of the simulated planets (1/40th fraction of the total, uniformly and randomly selected for the whole plane) overlay-ed by three shaded regions. These are:

(i) In the top green shaded region, planets are insensitive to the host star’s metallicity. For cold giants (§5.2) this is because these planets do not experience strong tidal forces at their far away locations. They hence eventually collapse independently of the presence of pebbles in the host disc. For hot very massive planets, a second collapse route – by radiative cooling – becomes available, which “saves” the fragments from tidal disruptions at low metallicities (§5.3).

(ii) In the red region, pebble accretion is most effective at preventing tidal disruptions at high metallicities, so there is a strong positive metallicity correlation (§5.1). Although we did not analyse this specifically, there is also a positive metallicity correlation for partially disrupted planets, e.g., with masses approximately between that of Neptune and Saturn, because these planets have very massive cores, and massive cores are assembled preferentially at high metallicity.

(iii) In the black shaded region, the metallicity correlation is complicated. If measured within a certain mass window, there is no clear correlation for the *number* of cores versus $[M/H]$. For example, cores with mass $M_{\text{core}} \approx 3 M_{\oplus}$ are relatively rare at low metallicities (since in this case most cores are less massive than that, see fig. 9), then abundant at \sim Solar metallicity, and are rare again at high metallicities, since most cores then become more massive than $3 M_{\oplus}$. However, there is an average core *mass correlation* with metallicities: the higher the metallicity, the more massive

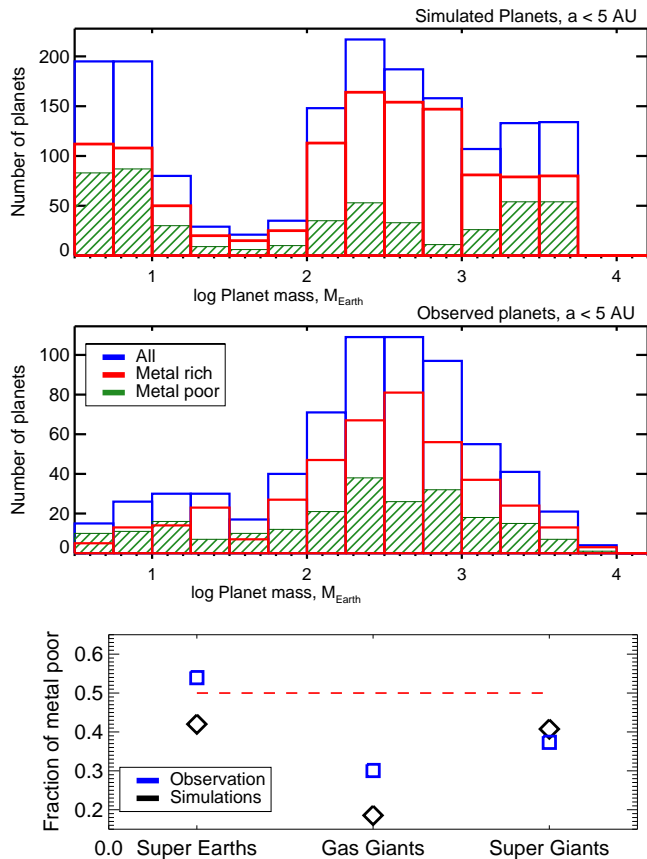


Figure 14. Mass function of simulated (top) and observed (middle) planets, sliced into the metal rich and metal poor samples. The bottom panel shows the fraction of planets that are metal poor for the three selected groups of planets, for both observation and simulation. No attempt to include errors or observational biases in this figure was made.

an average core. We called this type of correlation ”number neutral but mass positive” in §5.1.

It is tempting to compare these theoretical predictions to the observations. Observations of planets in the cold region are too incomplete for us to attempt a comparison, hence we limit our attention to the inner 5 AU region of the simulated planets. As we wish to compare this to observations, we included only planets with the stellar reflex velocity $v_* > 2$ m/s. This preferentially removes the planets less massive than \sim tens of M_{\oplus} from the simulated sample.

We have no access to a uniformly selected observed planet sample for the broad mass range to investigate metallicity correlations of the observed planets. Therefore, we only attempt a rather simple comparison here. We assume that metal-rich and metal-poor planets of same mass are affected roughly similarly by detection biases, and use the planets in the *exoplanets.eu* sample (Schneider et al. 2011). We select planets with measured masses and host-star separations less than 5 AU, and with the host star masses between $0.6 M_{\odot}$ and $1.5 M_{\odot}$.

We slice the populations of the simulated and observed planets into the metal poor ($[M/H] < 0$) and the metal rich ($[M/H] > 0$) samples. In fig. 14, the top panel shows

the PMFs for the simulated planets inside the inner 5 AU. The blue, the red and the hashed green histograms show the PMF for the total, the metal rich and the metal poor samples, respectively. The middle panel in fig 14 shows the observed sample of planets (cf. fig. 4), also sliced by the metallicity of the host. No attempt to include errors or observational biases in this panel was made. For this reason, the observed PMF shown in the bottom panel massively under-estimates the number of low mass planets which are much harder to detect than high mass ones. However, the ratio of the metal poor to metal rich systems at a given planet mass is probably much more robust, and this is what we intend to compare with the simulations.

The bottom panel of fig. 14 shows the fraction of stars that are metal poor for three mass groups of planets. Qualitatively, similar trends are seen in the simulations and in the observations: the Super-Earths are (number) insensitive to the host star metallicity, medium mass giants are positively correlated with the host star metallicity, and the most massive gas giants are somewhat weakly correlated with the metallicity. The highest mass bin in this picture is particularly interesting since, it appears to us, in CA the highest mass giants should still correlate with the metallicity. These planets are formed in CA by accreting more gas onto less massive giants, and those do correlate with z . There is thus a potential to distinguish CA and TD by the metallicity correlations for the highest mass gas giants.

As already mentioned, the observational sample for exoplanets used here is unfortunately not uniformly selected and may have various selection biases. Adibekyan et al. (2013) presented a study of metallicity correlations for planets selected in a much more homogeneous way from the SWEET-Cat database. Among a number of correlations, they find that most massive giants in their sample (more massive than $4 M_J$) correlate with metallicity weaker than less massive giants, although the statistical significance of this result is not very robust due to a small number of planets in the high mass bin.

6 ATMOSPHERES ON TOP OF CORES

As described in §2.2.3, in this paper we also calculate the mass of gas gravitationally bound to the cores inside the pre-collapse fragments. When the fragment is disrupted this atmosphere is assumed to survive, remaining bound to the core. This is a reasonable assumption, since the density of these atmospheres are typically higher than that of the main body of the fragment by orders of magnitude (e.g., cf. Nayakshin et al. 2014). The atmospheres could lose more mass after the fragment disruption by photo-evaporation if the remnant migrates sufficiently close to the star (e.g., Owen & Wu 2013); this post-disruption evaporation is not included in our calculations at this stage.

The top panel of figure 15 shows the ratio of the atmosphere mass to that of the core for the simulated planets in the inner 5 AU. Colours and types of the symbols indicate the host star metallicity, as before. We see that metallicity does not play a big role in establishing the mass of the atmosphere at a given M_{core} . The metallicity is more important in determining the core mass itself, as we saw in §5.1. One notices that metal rich systems (blue and red) appear more

often at $M_{\text{core}} \gtrsim 5 M_{\oplus}$ part of the figure, whereas the metal poor systems typically have smaller mass cores.

Notice that there is a large spread in the relative atmosphere mass at a given M_{core} . This spread is not a function of metallicity. The physical reason for the spread is that cores of a given mass can be born inside fragments of different masses and/or different evolution histories. These fragments have different central gas pressure and densities which explains why same mass cores may have different atmosphere masses as measured at the fragment disruption (see also Nayakshin et al. 2014). In addition, we parameterise the core’s luminosity by introducing the Kelvin-Helmholtz time for the core, t_{kh} , which is a Monte Carlo parameter varied between 10^5 and 10^7 years (see Table 1 and §2.2.3). Due to this, the luminosity of the cores vary, and that also imprints onto the scatter of the atmosphere’s mass at a given M_{core} .

With all the scatter, it is nonetheless clear that cores less massive than $\sim 5 M_{\oplus}$ do not possess atmospheres more massive than a few percent of the core, whereas cores more massive than that may have atmospheres of mass comparable to that of the core. A few of these formally had atmospheres more massive than the core, which we capped at $M_{\text{atm}} = M_{\text{core}}$ exactly as explained in §2.2.3. Physically in these cases we expect that a tidal disruption of the fragment will result in a partial disruption of the fragment only as there can be more mass in the collapsed atmosphere around the core than the core mass itself. At the same time, we note that in fig. 15 there are also quite massive core, $M_{\text{core}} \gtrsim 10 M_{\oplus}$ that have very small, $\sim 1\%$, atmospheres.

The bottom panel of fig. 15 shows the metallicity of the atmospheres of the cores, Z_{atm} . All of these values are strongly super-Solar ($Z_{\odot} = 0.015$). This is to be expected as gas fragments accrete pebbles in our model, so their abundances are super-Solar (cf. §8 on this for more detail). In addition to that, grains do sediment to the centre of the fragment and so the metal abundance in the atmosphere is usually even higher than the mean fragment metallicity (e.g., figure 9 in paper I shows that the metallicity is the highest in the centre of a planet).

7 ROCK DOMINATED COMPOSITION OF CORES

Figure 16 shows the ratio of the volatile (water and CHON) mass in the core to the total mass of the core, again for the four different metallicity groups. We see that with a few exceptions at the low core mass end, the cores are always dominated by the rocks rather than “ices”. This is especially true at the high core mass end, where CHON contribute a few % of the mass only.

This result is not particularly surprising in the light of previous studies of grain sedimentation inside the pre-collapse fragments. Helled & Schubert (2008) showed that water ice grains are unlikely to sediment into the cores of pre-collapse gas fragments of mass higher than about $1 M_{\text{J}}$ because the fragments are too hot for the icy grains to exist even at early times. Helled et al. (2008) then showed that organics (modelled as CHON) grains have somewhat better chances of sedimenting into the cores since their vaporisation temperatures are ~ 350 to 400 K, depending on gas pressure, whereas water ice vaporises above $T \sim 150 - 200$ K. Rocks

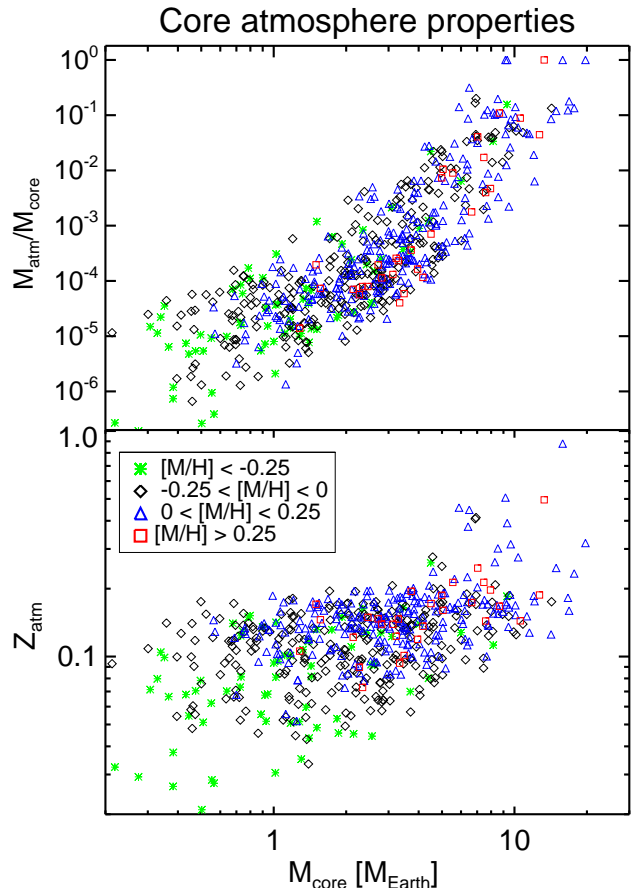


Figure 15. Top: the ratio of the mass of the bound atmosphere to that of the core as a function of core mass after the fragment disruption. Bottom: the metallicity of the atmospheres shown in the top panel. The legend explains the meaning of the symbols.

and Fe (counted together as one species in our paper) are thus the main components of which the cores are made in the TD model (see also Forgan & Rice 2013).

There remain *quantitative* uncertainties in the composition of the cores. We here chose a rather low initial temperature for the fragments, so that water ice can sediment initially in gas fragments less massive than a few Jupiter masses. This is why there are some volatile grains in the relatively low mass cores in fig. 16. However, high mass cores require a long, \gtrsim a few 10^4 years, assembly time. The fragments containing those heat up to temperatures of hundreds of K during this time, so that neither CHON or water ice grains can sediment.

This prediction of the model is important as it is very different from CA model in which massive cores have the best chance of growing beyond the ice line where water ice can sediment, so that they are dominated by ices.

8 METAL OVERABUNDANCE OF GAS GIANTS COMPOSITION

Gas giant planets, and also their less massive cousins, are over-abundant in elements heavier than H/He com-

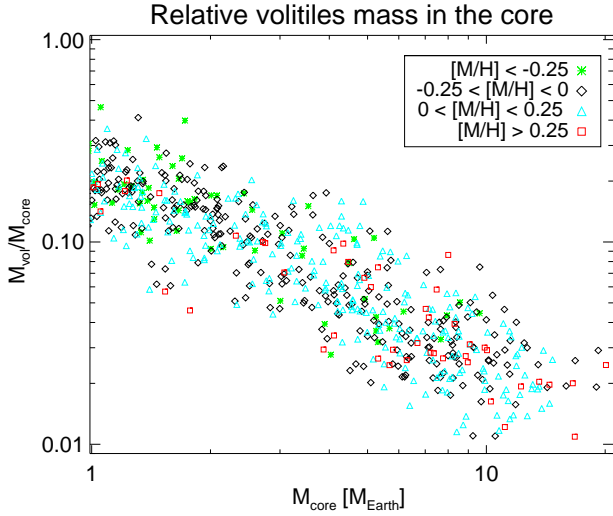


Figure 16. The ratio of the core mass in the volatiles (water ice and CHON) to the total mass of the core as a function of the core mass. Note that high mass cores are strongly dominated by rocks in our model, in contrast to CA.

pared with their host stars. This is well known for the Solar System planets (e.g., Guillot et al. 2004) and is now also robustly established for exoplanets at close separations (Miller & Fortney 2011). This important fact is usually used (e.g., Helled et al. 2013) to argue that the CA model is a clear favourite to explain giant planets formation because planets made by CA contain heavy cores which makes the planets more compact (as required by the observations) than they would be if they had their host star metallicities and did not contain massive cores. In contrast, GI planets may be enriched in metals by accretion of grains or planetesimals early on (Boley & Durisen 2010), but until recently it was thought that this enrichment is not fundamental to the survival of GI planets. It would thus seem that GI planets may have a range of metallicities – from sub-host values to many times the metallicity of the host (Boley et al. 2011).

However, as argued in Nayakshin (2015a), pebble accretion is the process that makes relatively low mass (a few M_J) GI fragments survival possible. Radiative cooling is too inefficient, and it is pebble accretion that allows these fragments to contract into the much denser “hot start” GI planet configurations so that they avoid tidally disruptions in the inner disc. Therefore, we may expect that the metallicity of TD giant planets is elevated compared to their host stars.

Figure 17 shows the ratio of the metallicity of the simulated planets in the inner 5 AU, Z_{pl} , to the metallicity of the host star as a function of the planet’s mass. As before, the population is broken into four bins by the host star metallicity, $[M/H]$, as indicated in the legend. In addition to that, we used the “mixed model” in Table 1 of Miller & Fortney (2011) to show their best estimates for such a ratio for their sample of observed giant planets. These models are shown with the blue symbols with the error bars in fig. 17.

Fig. 17 indicates that TD giant planets are indeed over-abundant in metals compared to their host stars. In addition, there is an anti-correlation between the “over-metallicity” ratio, Z_{pl}/Z_{star} , and the mass of the planet. The origin of this anti-correlation is slightly different for plan-

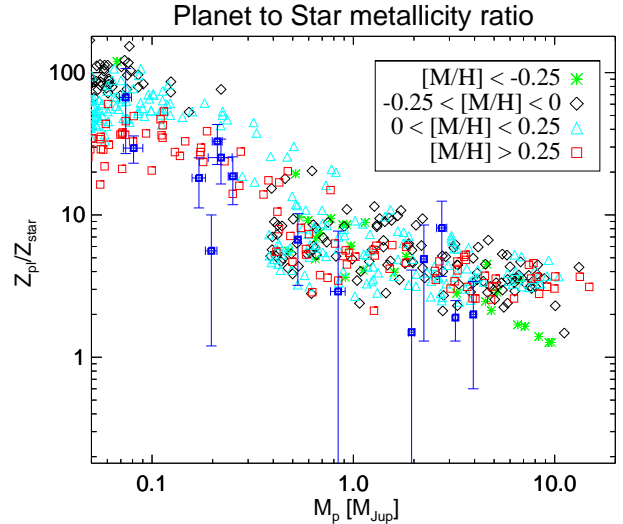


Figure 17. Ratio of metal abundance of the giant planets to that of their host star. The symbols with the error bars are models by Miller & Fortney 2011 based on observations of close-in but not strongly irradiated gas giant planets.

ets that did not experience tidal disruptions, $M_p \gtrsim 0.33 M_J$ here, and those that did (the less massive ones).

For the partially disrupted planets, the correlation is physically similar to that of CA gas giant planets. The metal content of these planets is actually dominated by the core’s mass, which is $M_{core} \sim 10 M_{\oplus}$. The atmosphere, while also over-abundant in metals as we saw in fig. 15, contains a minority of the metals mass. Since $M_{core} \sim \text{const}$, and is independent of the total planet mass, $Z_{pl} \sim M_p^{-1}$ is this regime.

For heavier planets that did not go through a tidal disruption, the correlation occurs because (a) higher mass planets are hotter to begin with (e.g., Helled & Schubert 2008; Nayakshin 2011) and (b) collapse faster as radiative cooling contributes more to their contraction (Nayakshin 2015a). Therefore, more massive gas fragments require a smaller fractional mass increase in pebbles to reach the central temperature of ~ 2000 K and collapse.

Note that we do not take into account gas accretion onto the planets in this paper in either pre- or post-collapse evolution. If this assumption was relaxed, post-collapse planets could gain mass by accretion of gas with metallicity close to that of the host star. This would therefore dilute their metallicity at a given total planet mass, but, importantly, would not change the downward trend that we see in fig. 17.

Our simulation results are qualitatively consistent with the models of Miller & Fortney (2011), although we did not fine tune any of the parameters to specifically address this issue. We finish this section reiterating what we said in §4.1.1: the present day bulk structure of the planets may not be uniquely indicative of the route that these planets formed. We believe TD is as promising as CA in explaining the bulk composition of Solar and extra solar planets.

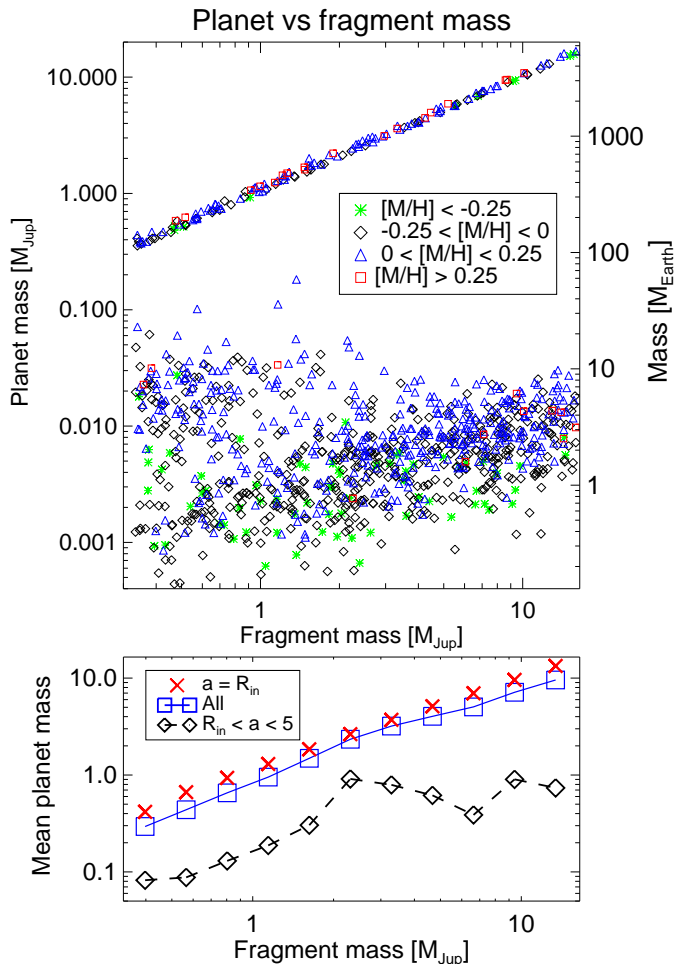


Figure 18. Top: Final mass of the planet versus the initial mass of the fragment. The meanings of the symbols is the same as in fig. 15. Bottom: Mean mass of the planets more massive than $5 M_{\oplus}$ versus initial fragment mass for three regions in the host-planet separations.

9 WHICH FRAGMENTS MAKE WHICH PLANETS?

One may wonder how the value of the initial fragment mass maps into the kind of planets that emerge in the end. To investigate that, the top panel of figure 18 shows the final mass of the planet versus the initial fragment mass, M_f , for a uniformly randomly chosen (7% of the total) subsample of all the planets in the simulations. The colours reflect the metallicity of the system, as before. The nearly straight line in the upper part of the panel are the fragments that avoided tidal disruption and collapsed into giant gas planets. Mass of these planets is close to the initial fragment mass, save for the addition of metals by pebble accretion; hence the (almost) one to one correspondence between the final and the initial planet masses.

The planets below that line are planets that went through a total or a partial gas envelope disruption. These are mainly rocky core planets with only a few systems that are dominated by gas, as we saw earlier.

This figure demonstrates that the mass of the core made within the fragment is not a unique function of the frag-

ment’s mass. In fact, the most massive cores are found in the least massive fragments, those below $M_f \sim 2 M_J$. This result is not new. Helled et al. (2008); Helled & Schubert (2008) showed that the more massive the fragment is, the less massive is the core made inside it during the pre-collapse phase. This is because the central temperature of pre-collapse fragment is believed to increase with its mass even at the initial stage due to adiabatic compression being stronger for more massive fragments (Masunaga & Inutsuka 2000; Nayakshin 2010b). Massive fragments also cool radiatively more rapidly, cutting the available time for the core’s growth. The exact value of the initial temperature, T_0 , is however difficult to calculate from first principles, especially in the case of the disc. In this paper we assumed that $T_0 \propto M_f^{1/2}$. A stronger dependence would make even smaller cores at high M_f than the top panel of figure 18 shows.

The bottom panel of fig. 18 presents the mean mass of the planet as a function of the initial fragment mass. This is calculated neglecting the least massive planets, $M_p < 5 M_{\oplus}$, assuming that these are unlikely to be detected due to selection bias. Further, three spatial regions are picked for this panel: the planets on the very edge of the disc (red crosses), planet found anywhere in the disc (blue squares) and planets found between the inner edge and 5 AU (black diamonds).

In general, we see that the mean mass of the resulting planet correlates positively with the mass of the initial fragment. This result is of no clear importance if the spectrum of initial fragment masses is same for all the systems studied – as assumed in this work. This may not necessarily be so, and further work on the gravitational fragmentation of discs is needed to study this issue. One rather likely outcome, however, is that the mass of the fragment would increase with the mass of the host star. If this is the case then the bottom panel of fig. 18 predicts that the mean mass of a planet would increase with the mass of the host star.

The most massive cores, $M_{\text{core}} \sim 10 M_{\oplus}$ are made in relatively low mass fragments, $M \lesssim 2 M_J$, as emphasised before. We can hence expect a similar result for massive atmospheres *bound* to the core. Fig. 19 indeed shows that cores with massive atmospheres are only made in low mass fragments. This result is interesting in that it predicts that in environments in which only massive fragments are born in the disc, there is very little chance of finding any planet with mass intermediate between a few Earth masses and a few Jupiter masses. Fig. 19 shows the mass of the atmosphere irrespectively of whether the fragment is disrupted, in which case the atmosphere remains bound to the core, or collapses, in which case the “atmosphere” simply becomes the part of the much more massive gaseous envelope of the planet.

10 RADIAL DISTRIBUTION OF PLANETS

We finally discuss the distribution of the simulated planets over the planet – host separations. This is one of the most interesting observables. Unfortunately it is also one of the most uncertain results of our model at this point. While many of the planet properties studied in previous sections, including the metallicity correlations, depend mainly on the planet formation processes of TD (fragment forma-

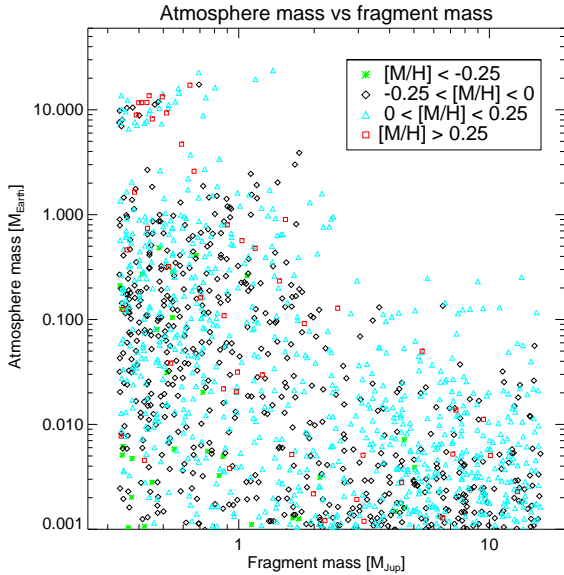


Figure 19. Mass of the core’s atmosphere versus the fragment’s initial mass. Note that all fragments, whether disrupted or not, are plotted. For non-disrupted fragments the atmosphere simply becomes the part of the much larger gaseous envelope and is not distinguishable from it.

tion, contraction, core growth, tidal disruption, etc.), the radial distribution of planets depends at least as sensitively on the protoplanetary disc evolution model accepted here. Section 10.4 shows why this statement is true for our simulated models, but it is also bound to be true for any planet formation theory (e.g., Alexander & Armitage 2009). These uncertainties go beyond planet formation theory and cannot be resolved until evolution of protoplanetary discs is understood in sufficient detail. We believe that real protoplanetary discs are far more complex than the simple model accepted here or in any other published population synthesis models (e.g., Ida & Lin 2004a,b, 2008; Mordasini et al. 2009a, 2012). This view is motivated by the increasingly popular ideas of episodic accretion on young stars (e.g., Dunham & Vorobyov 2012) that may have direct connections to GI model (Boley et al. 2010; Nayakshin & Lodato 2012), and observational surprises in the population of “transition discs” that were expected to be the link between protoplanetary and debris discs (see the end of the Discussion section).

With this caveat in mind, fig. 20 shows how the planet final separations are distributed for four different groups of planets. The top panel (a) shows “Earths”, planets with mass $0.3 M_{\oplus} < M_p < 2 M_{\oplus}$. Panel (b) shows Super Earths defined to be planets with mass $2 M_{\oplus} < M_p < 15 M_{\oplus}$. The third and the fourth panels show “giants” with mass between $50 M_{\oplus}$ and $5 M_J$. Most massive gas giants, $M_p > 5 M_J$, are shown in panel (d). The histograms are further broken into the metal rich (red), the metal poor (green shaded) and the total populations (blue colour). We do not show in fig. 20 the “assimilated” group of planets, that is those that migrated all the way to $a = R_{in}$, since we cannot constrain their further fate here.

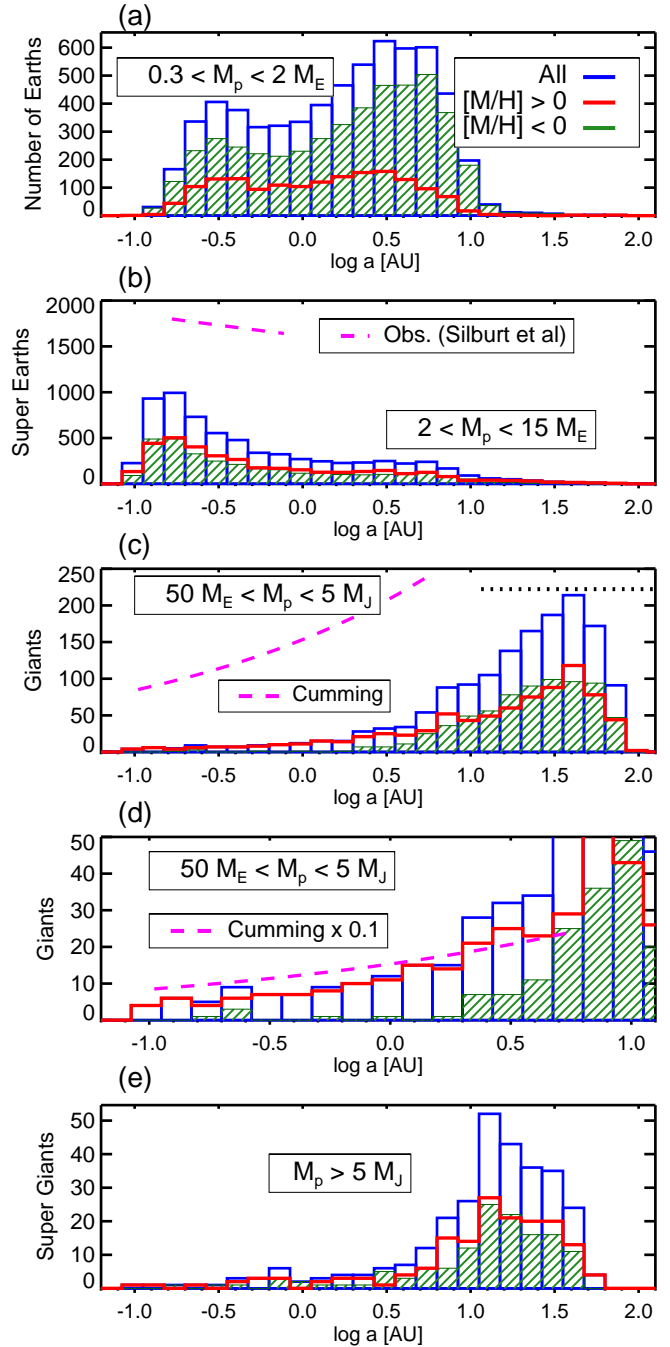


Figure 20. The histogram of planet final separations for four groups of planets: Earths, Super Earths, Giants and Super Giants, from top to bottom. The colours show all, metal rich and metal poor populations, as indicated in the legend on the top panel.

10.1 Low mass cores

Panel (a) of fig. 20 shows that Earth-like core-dominated planets are most abundant at $a \sim$ a few AU separations. Physically, this is because fragments migrating from the outer disc are disrupted most frequently in this region (this can be deduced already from simple analytical estimates, see, e.g., Nayakshin 2010a), and hence this is where these cores are deposited by the disruptions. Low mass cores do not migrate inward significantly, so they form the dominant

peak in the same spatial region. One also observes that the histogram for the low mass rocky planets is mainly composed of cores born at low metallicity environments, which is to be expected given the results of §5.

One may also note that the metal rich population of low mass cores forms a flatter distribution of host – planet separations which is shifted a little closer to the star. This can be attributed to two effects. Firstly, the cores born in metal rich environments are born in more compact gas fragments. These fragments are disrupted closer to the host star. Secondly, cores around metal rich stars are more massive on average than those in the low metallicity discs, and so they also migrate further in.

10.2 Super Earths

Panel (b) in fig. 20 indicates that super Earth planets are shifted towards smaller separations with respect to the low mass cores. This is due to a higher inward migration speed of the super Earths which brings most of them into the inner region. For this reason the super Earths dominate the mass function at small separations, as was already seen in fig. 6. The metal rich and the metal poor populations of the super Earths are quite similar, which again shows that there is no metallicity correlation for these planets.

Silburt et al. (2015) reconstructed the frequency of occurrence of *Kepler* detected planets in the size range $1-4R_{\oplus}$ in the orbital period range from ~ 10 to 200 days. The dashed purple line in panel (b) in fig. 20 shows their result, which should approximately map to the mass range we use for this panel. We see that there is a discrepancy of about a factor of three between the observations and our one fragment simulations. Another way of putting this is to say that if different fragments did not interfere with each other (which is most likely not true), then we would need ~ 3 fragments per star to reproduce the observed abundance of super Earths inside the inner ~ 1 AU.

We note that the outer region of \sim tens of AU contains very few cores in our simulations (see also fig. 2). This outcome stems from tidal disruptions of fragments becoming possible only in the inner $\lesssim 10$ AU region. This result does depend on assumptions and parameters of the model, such as the fragment migration speed, pebble abundance in the disc, the initial disc mass, etc. For example, simulations in paper II did produce massive cores in the outer tens of AU region (cf. fig. 4 in that paper).

10.3 Gas giants

Panels (c) and (d) of fig. 20 show the same simulated population of planets with mass between $50M_{\oplus}$ and $5M_J$, except panel (d) is a zoom-in on the inner 10 AU part of the histogram. These panels show that very few of the gas giant planets actually end up in the region between $0.1 < a \lesssim 5$ AU. The most common outcome (cf. also fig. 3b) for the initial fragments is to migrate inward rapidly and be destroyed or to collapse but end up on the inner edge of the disc at $a = 0.09$ AU. The next most common outcome is that some fragments are “stranded” in the outer region by the disc disappearing more rapidly than the fragments can migrate.

The fraction of the simulated gas giants in the inner disc appears too low compared with the observations. Cumming et al. (2008) show that the occurrence rate of gas giant planets with period less than 5.5 years and in the mass range $0.3M_J$ to $10M_J$ is $\approx 10\%$. The frequency of the observed giants around FGK stars from Cumming et al. (2008) is shown in panel (c) of 20 with the purple dashed line.

Biller et al. (2013) places a model-dependent upper limit of $\sim 10\%$ on the frequency of $1-20M_J$ directly imaged mass planets at separations $10-150$ AU. This shows that systems such as HR 8799 are very rare. Assuming a flat in $\log a$ distribution for such planets, we plot the Biller et al. (2013) result as a black dotted line (recalling that we have 20,000 host stars in our simulations).

Panel (c) shows clearly that while our model is marginally consistent with the upper limits on the directly imaged planets, the number of planets in the inner ~ 10 AU is very much smaller than observed. Physically, this is due to a very rapid inward migration of the giant planets through this region on the way to $a = R_{\text{in}}$, due to which it is quite unlikely that a planet would stop there at the time when the disc is dissipated away.

The zoom-in on the inner part of panel (c) is shown in panel (d). It shows that the fraction of medium mass giant planets in our sample (which is about 1.0 %) is almost exactly 10 times lower than the observed gas giant fraction (the purple dashed curve in panel [d] is same as in panel [c] but is multiplied by the factor of 0.1).

Evidently, the simulations could be reconciled with observations by either a different disc model which would have the planets migrate slower through the inner region, or by having ~ 10 fragments per host star initially and removing the “excess” far away giants by some process. Close planet-planet scattering during the formation phase (Vorobyov & Basu 2013) and stellar interactions may remove some of the far-out giants (Davies et al. 2014), but it seems doubtful that these processes would be effective in removing as much as 90% of the original population.

One feature in the radial distribution of gas giant exoplanets not reproduced by power-law fits such as that by Cumming et al. (2008) is the sharp “pile-up” of planets at $a \gtrsim 1$ AU Wright et al. (2009). Models by Alexander & Pascucci (2012) show that photo-evaporation of the disc may produce a similarly strong pile-up of planets at about the right place. Physically, when the disc is dissipated by photo-evaporation, the gas is removed most rapidly from the region with $R \sim$ a few AU, which then implies that the planets migrate through this region slower than one would expect from a non photo-evaporating disc. This then forms a spike on the final semi-major distribution of gas giants. Note that this physics is independent of how the gas giant planets are formed, although there is a strong dependence on the timing of the planet “injection” into the inner few AU of the disc.

Although our models include disc photo-evaporation, we do not find such a strong pile-up of gas giants in our calculations. However, further tests, to be presented elsewhere, show that pile-up formation is a strong function of the disc viscosity parameter α_0 . In this paper we kept it at a fixed “reasonable” value $\alpha_0 = 0.005$ (cf. §2.2.1). Simulations with a broad range of α_0 actually do result in a cliff-like decrease

of gas giants inward of $a \sim 1$ AU. We plan to analyse and present this issue in future work.

Finally, panel (e) of fig. 20 shows the radial distribution of planets more massive than $5 M_J$. As for less massive planets, most of these are located at large separation. There is no strong metallicity correlation either in the inner or the outer disc for these planets.

10.4 Disc evolution impact on planet yields

As can be gathered from §2.2.1 and §2.2.4, even with a fixed radial structure of our initial discs and a small – only a factor of two – range in the initial total disc mass, the time scale for the protoplanetary disc dissipation varies widely between the runs in line with the observed range in the disc lifetimes (fig. 1). It may be expected that the duration of the disc lifetime has a significant impact on how the fragments evolve. To explore this issue, we define an “evaporation time”, which is an estimate of the time scale on which the protoplanetary disc would be removed by photo-evaporation,

$$t_{\text{ev}} = \frac{M_d}{\dot{M}_{\text{ev}}}, \quad (9)$$

where M_d and \dot{M}_{ev} are the initial disc mass and the total photo-evaporation rate, respectively. We then define the planet yield as the frequency of a given type of planet formation for four planet sub-samples: hot giants at the inner disc edge, e.g., all planets more massive than $50 M_{\oplus}$ with the final planet-host separation $a = R_{\text{in}}$; hot and cold giants – same mass range but $R_{\text{in}} < a < 5$ AU and $a > 10$ AU, respectively; and hot sub-giants, $R_{\text{in}} < a < 5$ AU and $M_p < 25 M_{\oplus}$. The exact dividing masses are not important for what follows.

Figure 21 shows how the planet yields vary with the evaporation time. The meaning of the trends are physically clear. The faster the disc is evaporated, the smaller is the chance of a gas giant planet being “stranded” in the outer disc. In the limit of no photo-evaporation, $t_{\text{ev}} \rightarrow \infty$, our discs always manage to push the gas giants into the inner disc. Discs that are removed very quickly (short t_{ev}), on the other hand, disappear sooner than they are able to push the planet close to the star. For shortest t_{ev} bins, most of the initial fragments end up as cold giants.

For the hot giant planets the trend is not monotonic. At short t_{ev} , the longer the disc is present, the more of the cold giants end up closer to the star, hence the yield of the hot gas giants increases as t_{ev} increases. However, this upward trend levels off and then turns into a decreasing one at longer t_{ev} since then the hot giants are more likely to be pushed all the way to $a = R_{\text{in}}$, which is clear from the dashed blue curve, or be disrupted and become a sub-giant planet (the green dot-dash curve).

Figure 21 demonstrates that the outcome of planet formation process in the context of TD hypothesis for planet formation strongly depends on the disc model accepted, and this dependence is quite varied and may be non monotonic for different types of planets. While more experiments with different disc models are needed, it appears likely to us that the fraction of the cold giants formed in our models may be reduced by reducing the maximum photo-evaporation rate in our models (which is indeed very high, e.g., $\max[\dot{M}_{\text{ev}}] =$

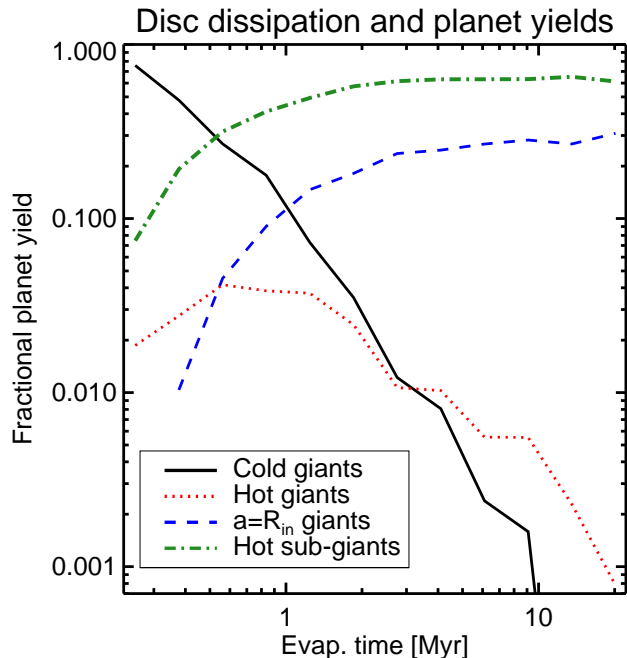


Figure 21. The frequency of cold and hot giant and hot sub-giant planet formation in our full simulated planet sample versus the estimated disc photo-evaporation time. The longer the disc exists, the smaller the chance of a cold giant planet formation, and the higher the chance that either a super-earth planet forms or that the gas giant is pushed all the way into the star ($a = R_{\text{in}}$).

$3 \times 10^{-7} M_{\odot} \text{ yr}^{-1}$). We therefore do not consider the mismatch in the radial distribution of our simulated planets as an unsurmountable challenge to the TD model.

11 DISCUSSION

This paper presented a synthesis of 20,000 planet formation experiments in the context of a relatively young planet formation theory called Tidal Downsizing. TD planet formation process begins as in GI model, with formation of a massive gas fragment in the outer self-gravitating gas disc. Instead of stopping there artificially, TD continues with (a) migration of the fragment in, as found in a dozen independent numerical simulations; (b) grain sedimentation forming the massive solid core in the centre of the fragment; (c) either collapse of the fragment, which results in a very young gas giant planet, or tidal disruption of the fragment once it migrated too close to the host star, which forms a core-dominated planet. TD model is thus GI plus modern physics, and is an attempt to rectify a certain injustice that GI model suffered while attention of the modellers in the last decades was focused on CA almost entirely.

The most important result following from our calculations is that many of the observed properties of the Solar System planets and exoplanets that were previously claimed to support CA theory uniquely are naturally reproduced by the TD theory as well. In particular, we find that

(i) giant planets do contain massive cores (§9). Their mass is dependent on the dust growth and sedimentation physics and the initial conditions for the fragments. At this point

we cannot rule out nearly zero core masses for some giant planets, especially for those more massive than a few M_J , since they contract rapidly and may vaporise their grains too soon (cf. also Helled & Schubert 2008). The most massive cores formed in the simulations are $\sim 10 - 20 M_\oplus$ (fig. 6);

(ii) gaseous envelopes of gas giants are strongly enriched in metals compared with their host stars (especially in organics and water since rocks are more efficient in sedimenting into the core), see §7;

(iii) the over-metallicity of gas giants decreases as the planet mass increases, as observed for the Solar and some giant exoplanets (§8);

(iv) the model is able to produce copious core-dominated planets with mass from sub-Earth up to $\sim 20 M_\oplus$. These planets are the most frequent outcome of TD planet formation hypothesis, but less so at high metallicities when giant planet survival becomes much more likely (cf. fig. 3b);

(v) a positive correlation of frequency of appearance of gas giant planets with metallicity of the host star for moderately massive giants in the inner ~ 5 AU region (cf. §§5 and 5.1).

(vi) Same planets do not show a metallicity preference at large separations ($a > 5 - 10$ AU) from their host stars (§5.2);

(vii) The most massive giant planets do NOT correlate positively with metallicity (cf. §5.3). Also, extending the results of §8 into the higher mass regime, BDs and low mass stellar companions formed by GI of their discs (and then having accreted more gas from it) have no physical reason to be over-abundant in metals compared with their host stars;

(viii) Core-dominated planets show a complicated pattern of occurrence versus the host star metallicity dependence. While the average core mass increases with metallicity, the number of the cores formed in the disc does not (§5.1). The latter is directly connected with the fact that more initial gas fragments survive at high metallicities, which implies fewer tidal disruptions, and hence fewer core-dominated planets. Sub-Neptune mass planets thus correlate in mass but not in numbers with the host star metallicity. We emphasise that this prediction stems from the basic mechanics of assembly of different types of planets in TD, e.g., more tidal disruptions equals less gas giants but more core-dominated planets. It is hence very robust, unlike the CA result that depends on detail of type I migration prescriptions (Mordasini et al. 2012);

(ix) the composition of simulated cores is dominated by rock and Fe, not ices, especially at high core mass end (§7). This prediction is significantly different from CA model. To remind the reader, core compositions are currently far from a settled issue even in the Solar System: while Uranus and Neptune are often referred to as "ice giants", there is no direct evidence that their bulk composition contains dominant amounts of ice. Modelling of *Voyager* and other data for these planets with a wide range of equations of state shows that compositions of these planets *could be* dominated by pure rock not ice (see Helled et al. 2011);

(x) due to a variety of fragment evolution histories, there is no one-to-one relation between the atmosphere mass and the core mass for the simulated planets. However, in general, the masses of the atmospheres of core-dominated planets are a tiny fraction of the total planet mass for cores less massive than $M_{\text{core}} < 5 M_\oplus$, but become comparable to the core's

mass for $M_{\text{core}} \gtrsim 5 - 15 M_\oplus$ (§6). The atmospheres are also metal-rich (fig. 15);

(xi) the planet mass function is dominated by the sub-Neptune mass planets, and contains a pronounced "tidal disruption desert" between $M_p \sim 20 M_\oplus$ and $M_p \sim 100 M_\oplus$ (cf. §4.1.1);

(xii) the planet mass function does not run away towards low mass ($M_{\text{core}} \lesssim 1 M_\oplus$) cores, unlike CA mass function (cf. §4.2.1).

(xiii) The PMF is smooth and does not divide on "rock-dominated" and "ice-dominated" cores (§4.2.2).

(xiv) The PMF has a rollover at mass $\sim 10 M_\oplus$ since it appears difficult to make more massive cores (§4.2.3).

Point (vii) may have significant implications beyond planet formation theories. It is usually said that formation scenarios of giant planets must be physically different from that of brown dwarfs and low mass stellar companions (e.g., see references in §2.1 of Winn & Fabrycky 2014), mainly because the metallicity correlations of these objects are different. While giant planet frequency of detection is positively correlated with metallicity of the host, for BDs such a correlation does not seem to exist conclusively, and for the low mass stellar companions it is the low metallicity hosts that are more likely to host the companion (Raghavan et al. 2010). We find that there may be physical reasons within the TD formation scenario that explain the divergent metallicity correlations for these different objects. In particular, if formation of planets starts with the birth of a $M_f \lesssim$ a few M_J gas fragment in a gravitationally unstable disc, and it does not grow more massive by gas accretion, then pebble accretion favours the survival of close-in exoplanets in high metallicity environments. If formation of BDs and low mass stellar companions starts with the birth of a more massive seed, e.g., $M_f \gtrsim 10 M_J$, then survival of these *by radiative cooling* is favoured at low metallicities (see also Helled & Bodenheimer 2011). We found this low-opacity mode of collapse to become important already at $\sim 10 M_J$ in §5.3, and it is clear that for higher mass fragments radiative cooling will dominate over the pebble accretion collapse even more.

If stellar mass secondaries can indeed grow from low mass $M_f \gtrsim 10 M_J$ seeds born in the early embedded phases of the star evolution, then there are further interesting implications stemming from TD model for the formation of planets in stellar binary systems. *Kepler* observations show that planets orbiting binary stars may be as common as $\sim 1-10\%$ (Welsh et al. 2012; Schwamb et al. 2013). This is surprising in the context of CA. Planetesimal velocity dispersions are whipped by the secondary in stellar binary systems (e.g., Paardekooper et al. 2008). Planetesimals are expected to collide in such systems at velocities from tens of m/s to ~ 1 km/s and fragment rather than grow (Paardekooper et al. 2012; Lines et al. 2014), making it challenging to explain the observed systems. In contrast, formation of these systems does not appear to strain any physical limits in TD but it does require the following chain of events to occur. In particular, suppose that several gas fragments are born in the outer disc, and one of them is much more massive than the rest and grows by gas accretion into a stellar secondary. It does not obviously precludes the other low mass gas fragments from maturing into planets although quantita-

tively their evolution is probably different from the one in a disc around a single star. The planet-mass fragments can be born inside or outside of the orbit of the more massive fragment. Formation of either circum-primary or circum-binary planets can then be achieved by shrinking the separations of the planet and/or the secondary due to the gravitational torques of the disc, assuming the disc is massive enough or is continued to be supplied with more matter from the outer envelope.

One feature of the model which is at odds with the observations is the radial distribution of the giant planets, with the ratio of cold (planet-host separation $a > 10$ AU) giants to warm giants ($a < 5$ AU) being larger than observational limits by a factor of 10 or more. Our simulations also did not reproduce the period valley (Wright et al. 2009) in that the observed one is between $0.1 \lesssim a \lesssim 1$ AU, whereas ours is from $0.1 \lesssim a \lesssim 5$ AU.

The number of far-out gas giants can be reduced if some of them self-destruct due to an overly luminous core, as in the proposed formation route for Neptune and Uranus by Handbury & Williams (1975), see also Nayakshin & Cha (2012). In addition, the radial distribution of giants is also very sensitive to the disc evolution model, e.g., the very poorly known disc viscosity parameter α , the locations of fragments birth, and also the very end phases of the disc dispersal (cf. §10.4). We believe that the current paradigm of protoplanetary disc evolution, which is the base of our disc model here, is unlikely to be entirely correct. This paradigm, developed with CA model in mind, all but discounts the importance of massive gas planets and brown dwarfs for the disc evolution, at best adding them post factum as an interesting but generally unimportant perturbers. The real picture is likely to be much more complicated as hinted by observations of “transition discs” (Andrews et al. 2011; Owen & Clarke 2012), with massive planets not only taking the mass from the disc but also giving it back when these objects are disrupted by tides from the host star (Nayakshin & Lodato 2012; Nayakshin 2013). This cannot possibly be added as a post factum perturbation to the disc evolution since the number of gas fragments born in the outer disc per star may be significant (e.g., Vorobyov & Basu 2006) and the total mass in these fragments during the overall disc lifetime be as much as $0.05 M_{\odot}$ or larger (Cha & Nayakshin 2011). This view joins up well with the developing paradigm of episodic accretion of young protostars in which all stars consume a number of massive clumps shipped into the star by disc migration from \sim hundreds of AU (Dunham & Vorobyov 2012; Audard et al. 2014; Vorobyov & Basu 2015).

12 CONCLUSIONS

Here we presented the third in the series paper on the population synthesis of planet formation experiments in the framework of the Tidal Downsizing (TD) model. A number of observed facts and correlations for exoplanet populations are reproduced by our model. On this basis we believe that TD model is a physically attractive alternative to CA in explaining many if not all of the observed exoplanets. We presented predictions for future observations that may distinguish this theory from CA. We hope that this work will

stimulate more theorists to contribute to the development of TD theory for planet formation.

13 ACKNOWLEDGMENTS

Theoretical astrophysics research at the University of Leicester is supported by a STFC grant. The authors acknowledge useful discussions with Richard Alexander and Vardan Adibekyan. This paper used the DiRAC Complexity system, operated by the University of Leicester, which forms part of the STFC DiRAC HPC Facility (www.dirac.ac.uk). This equipment is funded by a BIS National E-Infrastructure capital grant ST/K000373/1 and DiRAC Operations grant ST/K0003259/1. DiRAC is part of the UK National E-Infrastructure.

REFERENCES

- Adibekyan V. Z., Figueira P., Santos N. C., et al., 2013, *A&A*, 560, A51
- Alexander R. D., Armitage P. J., 2007, *MNRAS*, 375, 500
- Alexander R. D., Armitage P. J., 2009, *ApJ*, 704, 989
- Alexander R. D., Pascucci I., 2012, *MNRAS*, 422, L82
- Alibert Y., Carron F., Fortier A., et al., 2013, *A&A*, 558, A109
- Alibert Y., Mordasini C., Benz W., Winisdoerffer C., 2005, *A&A*, 434, 343
- Andrews S. M., Wilner D. J., Espaillat C., et al., 2011, *ApJ*, 732, 42
- Armitage P. J., Bonnell I. A., 2002, *MNRAS*, 330, L11
- Audard M., Ábrahám P., Dunham M. M., et al., 2014, *Protostars and Planets VI*, 387–410
- Baruteau C., Meru F., Paardekooper S.-J., 2011, *MNRAS*, 416, 1971
- Billar B. A., Liu M. C., Wahhaj Z., et al., 2013, *ApJ*, 777, 160
- Bodenheimer P., 1974, *Icarus*, 23, 319
- Bodenheimer P., Grossman A. S., Decamp W. M., Marcy G., Pollack J. B., 1980, *ICARUS*, 41, 293
- Boley A. C., Durisen R. H., 2010, *ApJ*, 724, 618
- Boley A. C., Hayfield T., Mayer L., Durisen R. H., 2010, *Icarus*, 207, 509
- Boley A. C., Helled R., Payne M. J., 2011, *ApJ*, 735, 30
- Boss A. P., 1997, *Science*, 276, 1836
- Boss A. P., 1998, *ApJ*, 503, 923
- Bowler B. P., Liu M. C., Shkolnik E. L., Tamura M., 2015, *ApJS*, 216, 7
- Buchhave L. A., Latham D. W., Johansen A., et al., 2012, *Nature*, 486, 375
- Cameron A. G. W., Decamp W. M., Bodenheimer P., 1982, *Icarus*, 49, 298
- Cha S.-H., Nayakshin S., 2011, *MNRAS*, 415, 3319
- Chambers J. E., 2014, *ICARUS*, 233, 83
- Clarke C. J., 2007, *MNRAS*, 376, 1350
- Crida A., Morbidelli A., Masset F., 2006, *ICARUS*, 181, 587
- Cumming A., Butler R. P., Marcy G. W., Vogt S. S., Wright J. T., Fischer D. A., 2008, *PASP*, 120, 531
- Davies M. B., Adams F. C., Armitage P., et al., 2014, *Protostars and Planets VI*, 787–808

- Donnison J. R., Williams I. P., 1975, *MNRAS*, 172, 257
- Dunham M. M., Vorobyov E. I., 2012, *ApJ*, 747, 52
- Fischer D. A., Valenti J., 2005, *ApJ*, 622, 1102
- Forgan D., Rice K., 2011, *MNRAS*, 417, 1928
- Forgan D., Rice K., 2013, *MNRAS*, 432, 3168
- Galvagni M., Mayer L., 2014, *MNRAS*, 437, 2909
- Goldreich P., Tremaine S., 1980, *ApJ*, 241, 425
- Gonzalez G., 1999, *MNRAS*, 308, 447
- Guillot T., Stevenson D. J., Hubbard W. B., Saumon D., 2004, *The interior of Jupiter*, Cambridge planetary science, Vol. 1, Cambridge, UK: Cambridge University Press, 35–57
- Haisch Jr. K. E., Lada E. A., Lada C. J., 2001, *ApJL*, 553, L153
- Handbury M. J., Williams I. P., 1975, *AP&SS*, 38, 29
- Helled R., Anderson J. D., Podolak M., Schubert G., 2011, *ApJ*, 726, 15
- Helled R., Bodenheimer P., 2010, *ICARUS*, 207, 503
- Helled R., Bodenheimer P., 2011, *ICARUS*, 211, 939
- Helled R., Bodenheimer P., 2014, *ApJ*, 789, 69
- Helled R., Bodenheimer P., Podolak M., et al., 2013, *ArXiv e-prints*
- Helled R., Podolak M., Kovetz A., 2008, *Icarus*, 195, 863
- Helled R., Schubert G., 2008, *Icarus*, 198, 156
- Hori Y., Ikoma M., 2011, *MNRAS*, 416, 1419
- Howard A. W., Marcy G. W., Bryson S. T., et al., 2012, *ApJS*, 201, 15
- Hubickyj O., Bodenheimer P., Lissauer J. J., 2005, *ICARUS*, 179, 415
- Ida S., Lin D. N. C., 2004a, *ApJ*, 604, 388
- Ida S., Lin D. N. C., 2004b, *ApJ*, 616, 567
- Ida S., Lin D. N. C., 2008, *ApJ*, 685, 584
- Johansen A., Lacerda P., 2010, *MNRAS*, 404, 475
- Johansen A., Oishi J. S., Low M., Klahr H., Henning T., Youdin A., 2007, *Nature*, 448, 1022
- Kuiper G. P., 1951, in *50th Anniversary of the Yerkes Observatory and Half a Century of Progress in Astrophysics*, edited by J. A. Hynek, 357–+
- Lambrechts M., Johansen A., 2012, *A&A*, 544, A32
- Lambrechts M., Johansen A., Morbidelli A., 2014, *A&A*, 572, A35
- Lin D. N. C., Papaloizou J., 1979, *MNRAS*, 186, 799
- Lin D. N. C., Papaloizou J., 1986, *ApJ*, 309, 846
- Lines S., Leinhardt Z. M., Paardekooper S., Baruteau C., Thébault P., 2014, *ApJL*, 782, L11
- Lodato G., Rice W. K. M., 2005, *MNRAS*, 358, 1489
- Lodders K., 2003, *ApJ*, 591, 1220
- Marley M. S., Fortney J. J., Hubickyj O., Bodenheimer P., Lissauer J. J., 2007, *ApJ*, 655, 541
- Masunaga H., Inutsuka S.-i., 2000, *ApJ*, 531, 350
- Mayor M., Marmier M., Lovis C., et al., 2011, *ArXiv e-prints*
- McCrea W. H., Williams I. P., 1965, *Royal Society of London Proceedings Series A*, 287, 143
- Meru F., 2013, in *European Physical Journal Web of Conferences*, vol. 46 of *European Physical Journal Web of Conferences*, 7003
- Miller N., Fortney J. J., 2011, *ApJL*, 736, L29
- Mizuno H., 1980, *Progress of Theoretical Physics*, 64, 544
- Morbidelli A., Bottke W. F., Nesvorný D., Levison H. F., 2009, *Icarus*, 204, 558
- Mordasini C., Alibert Y., Benz W., 2009a, *A&A*, 501, 1139
- Mordasini C., Alibert Y., Benz W., Klahr H., Henning T., 2012, *A&A*, 541, A97
- Mordasini C., Alibert Y., Benz W., Naef D., 2009b, *A&A*, 501, 1161
- Mordasini C., Mollière P., Dittkrist K.-M., Jin S., Alibert Y., 2014, *ArXiv e-prints*
- Nayakshin S., 2010a, *MNRAS*, 408, L36
- Nayakshin S., 2010b, *MNRAS*, 408, 2381
- Nayakshin S., 2011, *MNRAS*, 413, 1462
- Nayakshin S., 2013, *MNRAS*, 431, 1432
- Nayakshin S., 2014, *MNRAS*, 441, 1380
- Nayakshin S., 2015a, *MNRAS*, 446, 459
- Nayakshin S., 2015b, *MNRAS*, 448, L25
- Nayakshin S., 2015c, *ArXiv e-prints*
- Nayakshin S., 2015d, *ArXiv e-prints* (1411.5264)
- Nayakshin S., Cha S.-H., 2012, *MNRAS*, 423, 2104
- Nayakshin S., Cha S.-H., 2013, *MNRAS*, 435, 2099
- Nayakshin S., Helled R., Boley A. C., 2014, *ArXiv e-prints*
- Nayakshin S., Lodato G., 2012, *MNRAS*, 426, 70
- Oberc P., 2004, *ICARUS*, 171, 463
- Ormel C. W., Klahr H. H., 2010, *A&A*, 520, A43
- Owen J. E., Clarke C. J., 2012, *MNRAS*, 426, L96
- Owen J. E., Clarke C. J., Ercolano B., 2012, *MNRAS*, 422, 1880
- Owen J. E., Wu Y., 2013, *ApJ*, 775, 105
- Paardekooper S.-J., Leinhardt Z. M., Thébault P., Baruteau C., 2012, *ApJL*, 754, L16
- Paardekooper S.-J., Rein H., Kley W., 2013, *MNRAS*, 434, 3018
- Paardekooper S.-J., Thébault P., Mellema G., 2008, *MNRAS*, 386, 973
- Perri F., Cameron A. G. W., 1974, *ICARUS*, 22, 416
- Pollack J. B., Hubickyj O., Bodenheimer P., Lissauer J. J., Podolak M., Greenzweig Y., 1996, *Icarus*, 124, 62
- Rafikov R. R., 2005, *ApJL*, 621, L69
- Rafikov R. R., 2006, *ApJ*, 648, 666
- Raghavan D., McAlister H. A., Henry T. J., et al., 2010, *ApJS*, 190, 1
- Rice W. K. M., Lodato G., Armitage P. J., 2005, *MNRAS*, 364, L56
- Safronov V. S., 1972, *Evolution of the protoplanetary cloud and formation of the earth and planets.*, Jerusalem (Israel): Israel Program for Scientific Translations, Keter Publishing House, 212 p.
- Schneider J., Dedieu C., Le Sidaner P., Savalle R., Zolotukhin I., 2011, *A&A*, 532, A79
- Schwamb M. E., Orosz J. A., Carter J. A., et al., 2013, *ApJ*, 768, 127
- Shakura N. I., Sunyaev R. A., 1973, *A&A*, 24, 337
- Silburt A., Gaidos E., Wu Y., 2015, *ApJ*, 799, 180
- Sousa S. G., Santos N. C., Mayor M., et al., 2008, *A&A*, 487, 373
- Stamatellos D., Herczeg G. J., 2015, *ArXiv e-prints*: 1503.05209
- Stamatellos D., Whitworth A. P., 2008, *A&A*, 480, 879
- Stamenković V., Noack L., Breuer D., Spohn T., 2012, *ApJ*, 748, 41
- Stevenson D. J., 1982, *P&SS*, 30, 755
- Udry S., Mayor M., Naef D., et al., 2000, *A&A*, 356, 590
- Udry S., Santos N. C., 2007, *ARA&A*, 45, 397
- Vazan A., Helled R., 2012, *ApJ*, 756, 90
- Vorobyov E. I., Basu S., 2006, *ApJ*, 650, 956

- Vorobyov E. I., Basu S., 2013, *Memorie della Societa Astronomica Italiana*, 84, 866
Vorobyov E. I., Basu S., 2015, ArXiv e-prints 1503.07888
Weidenschilling S. J., 1980, *Icarus*, 44, 172
Welsh W. F., Orosz J. A., Carter J. A., et al., 2012, *Nature*, 481, 475
Winn J. N., Fabrycky D. C., 2014, ArXiv e-prints
Wright J. T., Upadhyay S., Marcy G. W., Fischer D. A., Ford E. B., Johnson J. A., 2009, *ApJ*, 693, 1084
Youdin A. N., Goodman J., 2005, *ApJ*, 620, 459
Zhu Z., Hartmann L., Gammie C., 2009, *ApJ*, 694, 1045
Zhu Z., Hartmann L., Nelson R. P., Gammie C. F., 2012, *ApJ*, 746, 110